Experience with fitting of multi-technique observations

(with examples: QZ Car, δ Ori, β Lyr, (216))

1''

Hvar Stellar Meeting

M. Brož, P. Harmanec, D. Mourard, J. Budaj, A. Opištilová, K. Vitovský, ...

STRANGE CASE

OF

DR JEKYLL AND MR HYDE

BY

ROBERT LOUIS STEVENSON

LONDON
LONGMANS, GREEN, AND CO.
1886

Strange case of...

Dr. Vokrouhlický

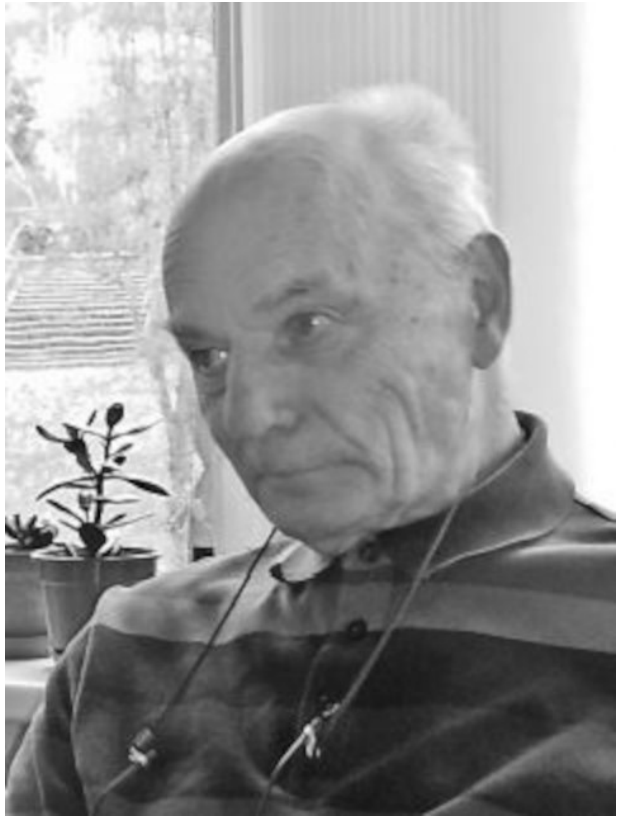

Mr. Mayer

"any similarity to actual persons is purely coincidental"

Model (Xitau)

+ SWIFT integrator
+ Kepler
+ N-body perturbations, ...
+ stability!
+ fitting of orbits
+ simplex

1. astrometry (SKY)
2. radial velocity (RV)
3. transit-timing variations (TTV)

Model (Xitau)

+ SWIFT integrator
+ Kepler
+ N-body perturbations, ...
+ stability!
+ oblateness
+ multipoles ($l = 10$)
+ parametrized post-Newtonian (PPN)
+ internal tides
+ external tides
– "brute-force"
– variable geometry
+ fitting of orbits
+ fitting of radiative parameters
– fitting of shapes
+ simplex
+ subplex
– annealing

1. astrometry (SKY)
2. differential astrometry (SKY2)
3. angular velocity (SKY3)
4. radial velocity (RV)
5. transit-timing variations (TTV)
6. eclipse duration (ECL)
7. visibility (VIS)
8. closure-phase (CLO)
9. triple product (T3)
10. light curve, u. Wilson-Devinney (LC)
11. light curve, u. polygonal (LC2)
12. synthetic spectra (SYN)
13. spectral-energy distribution (SED)
14. adaptive-optics silhouettes (AO)
15. adaptive-optics imaging (AO2)
16. occultations (OCC)

N-body
Levison & Duncan (1994)

$$\boldsymbol{f} = -\sum_{j \neq i}^{N} \frac{G m_j}{r_{ij}^3} \boldsymbol{r}_{ij} + \boldsymbol{f}_{\text{ppn}} + \boldsymbol{f}_{\text{oblat}} + \boldsymbol{f}_{\text{multipole}} + \boldsymbol{f}_{\text{tides}}.$$

PPN

Standish & Williams (2006)

$$\boldsymbol{f}_{\mathrm{ppn}} = \sum_{j \neq i}^{N} [-K_1 (K_2 + K_3 + K_4 + K_5 + K_6 + K_7 + K_8) \boldsymbol{r}_{ij} + K_1 (K_9 + K_{10}) \dot{\boldsymbol{r}}_{ij} + K_{11} \ddot{\boldsymbol{r}}_j],$$

$$K_1 = \frac{1}{c^2} \frac{G m_j}{r_{ij}^3},$$

$$K_2 = -2(\beta + \gamma) \sum_{k \neq i} \frac{G m_k}{r_{ik}},$$

$$K_3 = -(2\beta - 1) \sum_{k \neq j} \frac{G m_k}{r_{jk}},$$

$$K_4 = \gamma v_i^2,$$

$$K_5 = (1 + \gamma) v_j^2,$$

$$K_6 = -2(1 + \gamma) \dot{\boldsymbol{r}}_i \cdot \dot{\boldsymbol{r}}_j,$$

$$K_7 = -\frac{3}{2} \frac{(\boldsymbol{r}_{ij} \cdot \dot{\boldsymbol{r}}_j)^2}{r_{ij}^2},$$

$$K_8 = \frac{1}{2} \boldsymbol{r}_{ji} \cdot \ddot{\boldsymbol{r}}_j,$$

$$K_9 = (2 + 2\gamma) \boldsymbol{r}_{ij} \cdot \dot{\boldsymbol{r}}_i,$$

$$K_{10} = -(1 + 2\gamma) \boldsymbol{r}_{ij} \cdot \dot{\boldsymbol{r}}_j,$$

$$K_{11} = \frac{3 + 4\gamma}{2c^2} \frac{G m_j}{r_{ij}}.$$

multipoles
Burša et al. (1993)

$$U = -\frac{GM}{r}\sum_{\ell=0}^{N_{\rm pole}}\left(\frac{R}{r}\right)^{\ell}\sum_{m=0}^{\ell}P_{\ell m}(\cos\theta)[C_{\ell m}\cos(m\phi)+S_{\ell m}\sin(m\phi)],$$

$$\frac{\mathrm{d}U}{\mathrm{d}r} = -GM\sum_{\ell=0}^{N_{\rm pole}}R^{\ell}(-\ell-1)r^{-\ell-2}\sum_{m=0}^{\ell}P_{\ell m}(\cos\theta)[C_{\ell m}\cos(m\phi)+S_{\ell m}\sin(m\phi)],$$

$$\frac{\mathrm{d}U}{\mathrm{d}\theta} = -GM\sum_{\ell=0}^{N_{\rm pole}}R^{\ell}r^{-\ell-1}\sum_{m=0}^{\ell}P'_{\ell m}(\cos\theta)\sin\theta[C_{\ell m}\cos(m\phi)+S_{\ell m}\sin(m\phi)],$$

$$\frac{\mathrm{d}U}{\mathrm{d}\phi} = -GM\sum_{\ell=0}^{N_{\rm pole}}R^{\ell}r^{-\ell-1}\sum_{m=0}^{\ell}P_{\ell m}(\cos\theta)[-C_{\ell m}\sin(m\phi)m+S_{\ell m}\cos(m\phi)m],$$

$$\boldsymbol{f}_{\rm mp} = -\left(\frac{\mathrm{d}U}{\mathrm{d}r},\frac{1}{r}\frac{\mathrm{d}U}{\mathrm{d}\theta},\frac{1}{r\sin\theta}\frac{\mathrm{d}U}{\mathrm{d}\phi}\right),$$

$$C_{\ell 0} = \frac{1}{MR^{\ell}}\rho\int_V|\boldsymbol{r}|^{\ell}P_{\ell}(\cos\theta)\,\mathrm{d}V,$$

$$C_{\ell m} = \frac{2}{MR^{\ell}}\frac{(\ell-m)!}{(\ell+m)!}\rho\int_V|\boldsymbol{r}|^{\ell}P_{\ell m}(\cos\theta)\cos(m\phi)\,\mathrm{d}V,$$

$$S_{\ell m} = \frac{2}{MR^{\ell}}\frac{(\ell-m)!}{(\ell+m)!}\rho\int_V|\boldsymbol{r}|^{\ell}P_{\ell m}(\cos\theta)\sin(m\phi)\,\mathrm{d}V,$$

$$P_0(x)=1\,,\quad P_1(x)=x\,,\quad P_2(x)=\frac{1}{2}(3x^2-1),\ldots$$

$$P_{11}(x)=(1-x^2)^{\frac{1}{2}}\,,\quad P_{21}(x)=3x(1-x^2)^{\frac{1}{2}}\,,\ldots$$

tides
Mignard (1979)

$$\boldsymbol{f}_{\text{tides}} = K_1 \left[K_2 \boldsymbol{r}' - K_3 \boldsymbol{r} - K_4 (\boldsymbol{r} \times \boldsymbol{\omega} + \boldsymbol{v}) + K_5 (K_6 \boldsymbol{r} - K_7 \boldsymbol{r}') \right],$$

$$K_1 = \frac{3Gm^\star R^5 k_2 \Delta t}{(r' r)^5},$$

$$K_2 = \frac{5}{r'^2} \left[\boldsymbol{r}' \cdot \boldsymbol{r} \, (\boldsymbol{r} \cdot \boldsymbol{\omega} \times \boldsymbol{r}' + \boldsymbol{r}' \cdot \boldsymbol{v}) - \frac{1}{2r^2} \boldsymbol{r} \cdot \boldsymbol{v} (5(\boldsymbol{r}' \cdot \boldsymbol{r})^2 - r'^2 r^2) \right],$$

$$K_3 = \boldsymbol{r} \cdot \boldsymbol{\omega} \times \boldsymbol{r}' + \boldsymbol{r}' \cdot \boldsymbol{v},$$

$$K_4 = \boldsymbol{r}' \cdot \boldsymbol{r},$$

$$K_5 = \frac{\boldsymbol{r} \cdot \boldsymbol{v}}{r^2},$$

$$K_6 = 5\boldsymbol{r}' \cdot \boldsymbol{r},$$

$$K_7 = r^2,$$

$$\boldsymbol{\Gamma} = \boldsymbol{r} \times m' \boldsymbol{f}_{\text{tides}}.$$

Observables from coordinates

- SKY ... photocentric x, y
- SKY2 ... 2-, or 3-centric x, y
- SKY3 ... photocentric v_x, v_y
- RV ... barycentric v_z
- TTV ... barycentric z
- ECL ... heliocentric x, y
- VIS ... barycentric x, y
- LC ... heliocentric x, y, z
- OCC ... Earth, topocentric x, y, z
- cf. Jacobi elements a, e, i, Ω, ω, M
- cf. “times of interest”

```
Coordinate convention:

   y (as DE, N)

   ^    z (v_rad)
   |
   |  /
   | /
   |/
  -|----------> x (-RA, W)
   |

  internal

  (x, y) is plane-of-sky
  x positive towards W
  y positive towards N
  no reflections
  z radial, away from observer
```

Observables from coordinates (cont.)

- synthetic spectra: OSTAR, BSTAR, AMBRE, POLLUX, PHŒNIX, POWR, ...

$$L_j(T_{\mathrm{eff}\,j},\, R_j) = 4\pi R_j^2 \int_{\lambda-\Delta\lambda/2}^{\lambda+\Delta\lambda/2} F_{\mathrm{syn}}\,(\lambda,\, T_{\mathrm{eff}\,j},\, \log g_j,\, v_{\mathrm{rot}\,j},\, \mathcal{Z}_j)\,d\lambda;$$

$$I'_\lambda = \sum_{j=1}^{N_{\mathrm{bod}}} \frac{L_j}{L_{\mathrm{tot}}}\, I_{\mathrm{syn}}\left[\lambda\left(1 - \frac{v_{z\mathrm{b}j+\gamma}}{c}\right),\, T_{\mathrm{eff}\,j},\, \log g_j,\, v_{\mathrm{rot}\,j},\, \mathcal{Z}_j\right];$$

$$F'_V = \sum_{j=1}^{N_{\mathrm{bod}}} \left(\frac{R_j}{d}\right)^2 \int_0^\infty F_{\mathrm{syn}}\,[\lambda,\, T_{\mathrm{eff}\,j},\, \log g_j,\, v_{\mathrm{rot}\,j},\, \mathcal{Z}_j]\, f_V\,(\lambda)\,d\lambda,$$

- sphere vs. Roche (Lahey & Lahey 2015)
- cf. http://sirrah.troja.mff.cuni.cz/~mira/xitau/

ten Brummelaar etal. (2005)

Fringes

- $D = 1$ m, $B = 100$ m, $\lambda = 550$ nm, o. of a disc, $\theta = 1$ mas, no seeing, no $\Delta\lambda_{\mathrm{eff}}$, ...
- a drop in *visibility* (contrast) of fringes, i.e., the goal!

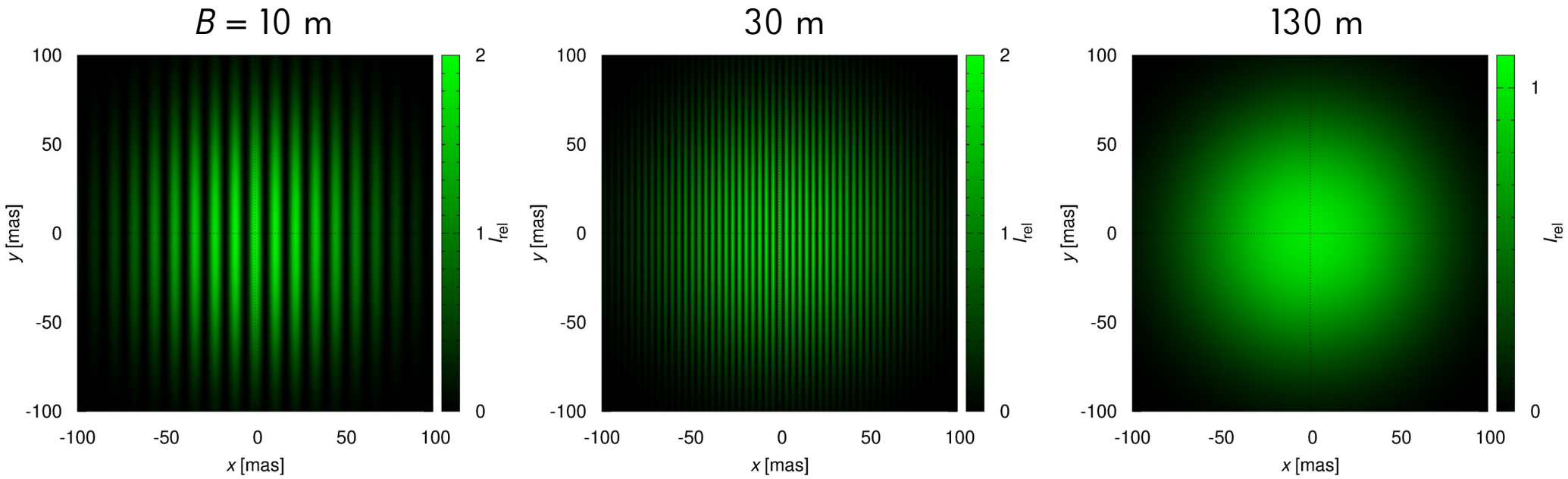

Fringes (cont.)

- delay line, periscopes → rearrangement of pupils (***B*** vs. ***b***) → constant # of f.

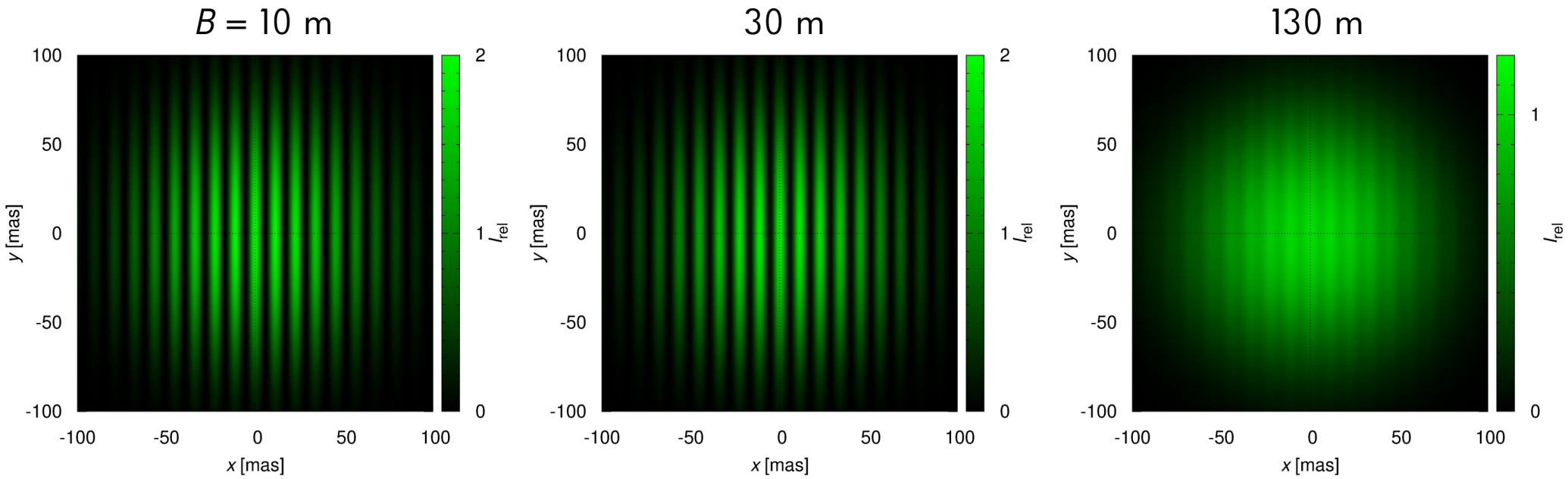

Fringes (cont.)

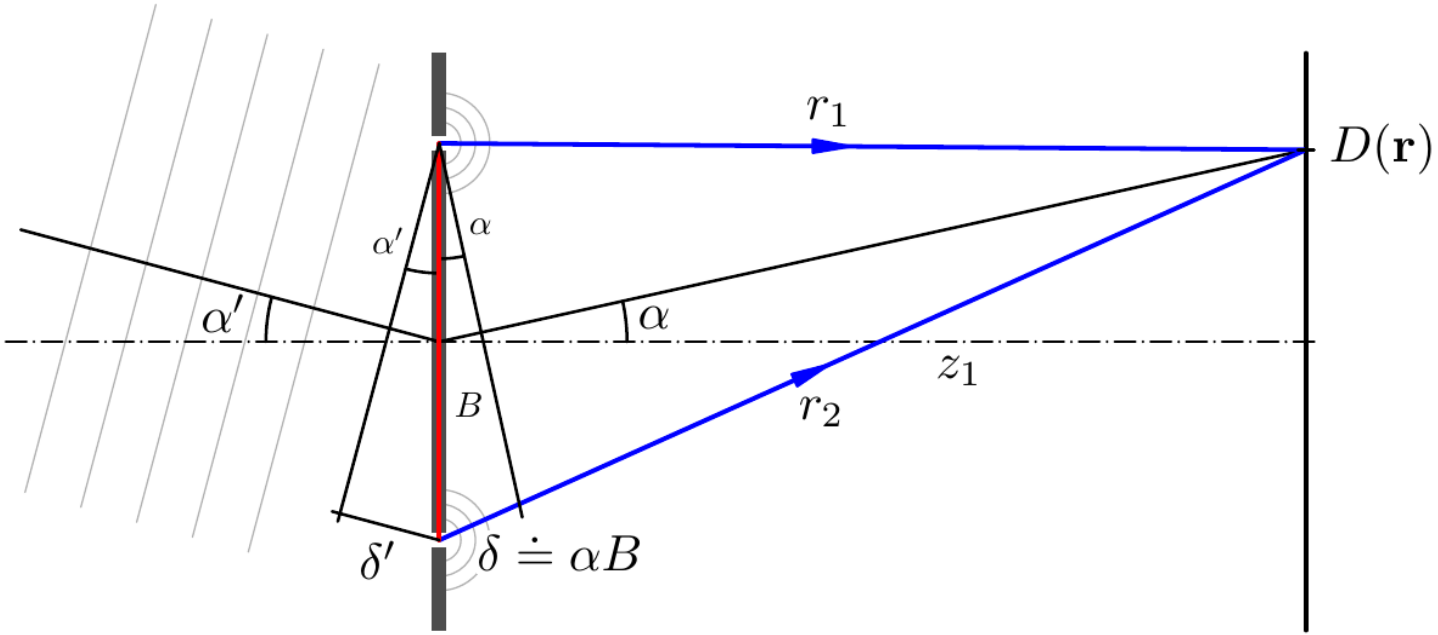

Obrázek 6.51: Uspořádání Youngova experimentu, kde B označuje vzájemnou vzdálenost štěrbin (základnu), z_1 vzdálenost stínítka od překážky, r_1, r_2 vzdálenost studovaného místa na stínítku od štěrbin, α odpovídající odchylka od osy překážky, α' úhel dopadu vlny na překážku, δ, δ' dráhové rozdíly vznikající za a před překážkou.

van Cittert-Zernike theorem

- intensity I [1], angles α, α' [rad], wave number $k = 2\pi/\lambda$ [m^{-1}], baseline B [m]

$$I(\alpha, \alpha') = I_0\{1 + \cos[k(\alpha + \alpha')B]\}\,, \tag{6.156}$$

$$I(\alpha) = \int I(\alpha, \alpha')\mathrm{d}\alpha' = \overbrace{\int I(\alpha')\mathrm{d}\alpha'}^{= I_0} + \overbrace{\int I(\alpha')\cos[k(\alpha + \alpha')B]\mathrm{d}\alpha'}^{= \Re[\mathrm{e}^{\mathrm{i}k\alpha B}\int I(\alpha')\,\mathrm{e}^{\mathrm{i}k\alpha' B}\,\mathrm{d}\alpha']}\,, \tag{6.158}$$

$$I(\vec{\alpha}) = I_0\left\{1 + \Re\left[\mu(\vec{B})\,\mathrm{e}^{-\mathrm{i}k\vec{\alpha}\cdot\vec{B}}\right]\right\}\,, \tag{6.159}$$

$$\mu(\vec{B}) \equiv \frac{\int I(\vec{\alpha}')\,\mathrm{e}^{-\mathrm{i}k\vec{\alpha}'\cdot\vec{B}}\,\mathrm{d}\alpha'}{I_0}\,, \tag{6.160}$$

Interferometric observables

- complex visibility $\mu = F(I)$
- squared visibility $V^2 = \mu\mu^*$
- phase arg μ
- triple product $T_3 = \mu_{12}\ \mu_{23}\ \mu_{31}$
- closure phase arg T_3
- triple product amplitude $|T_3|$
- differential visibility $\Delta V = \mu_{\lambda 1}\ \mu_{\lambda 2}^*$, approx. $V_{\lambda 1} \sim V_{\text{contiuum}}$ (cf. Mourard et al. 2009)
- differential visibility amplitude $|\Delta V|$
- differential phase arg ΔV
- estimator $C_1 = 2E_{\text{fringe}}/E_{\text{speckle}}$, $E \equiv \int W \mathrm{d}f$ (Roddier & Lena 1984, Mourard et al. 1994)
- estimator $C_2 = 2W_{\text{fringe}}(f)/W_{\text{speckle}}(f - B/\lambda)$
- cross-spectrum $W_{12} = \langle F(I_{\lambda 1})\, F(I_{\lambda 2})^* \rangle$ (Berio et al. 1999, 2001)
- ...

Interferometric observables

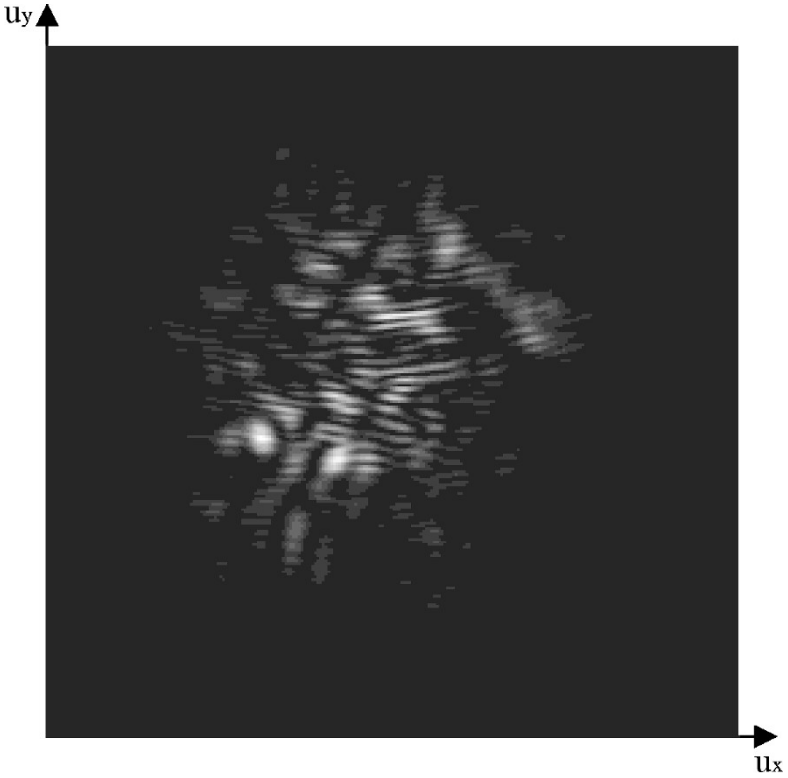

Berio et al. (1999)

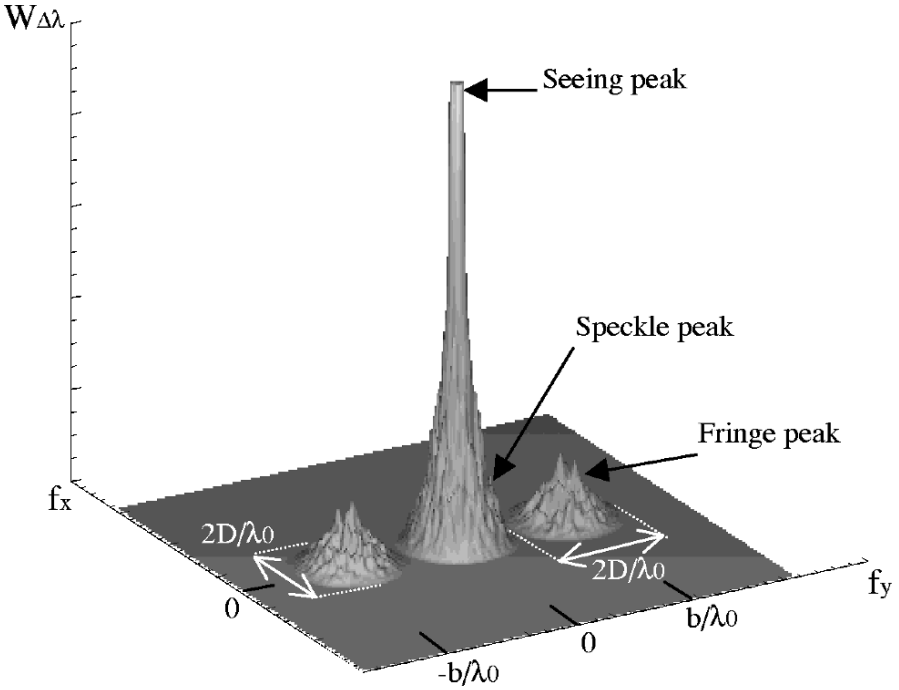

Fig. 1. Top, numerically simulated GI2T interferogram in the multichromatic mode and bottom, the corresponding spectral density. The fringe peaks are centered at $\pm b/\lambda_0$ because of the pupil rearrangement. (Coordinates are in arbitrary units.)

Simple i. models

- binaries, multiple *, uniform disk(s), limb-darkened d., ring, ... cf. combinations!

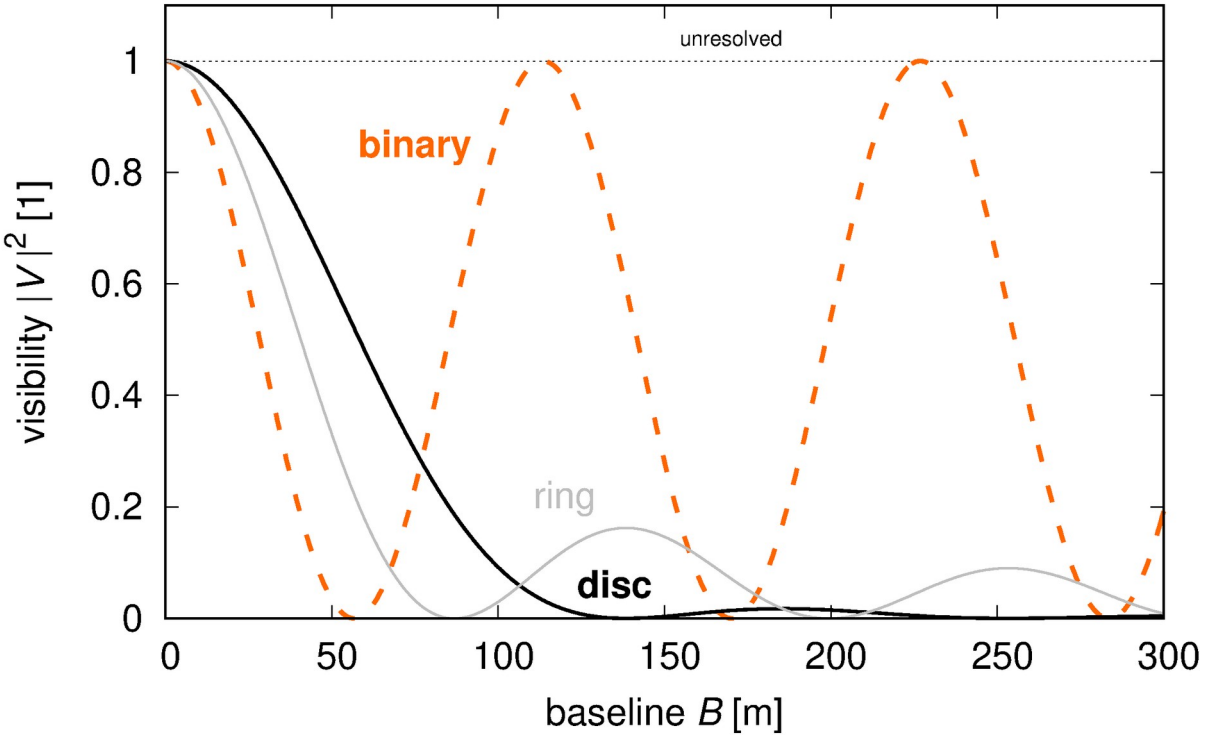

Complex i. models

- synthetic image $I(\alpha_x, \alpha_y)$ → Fourier transform → s. complex visibility $\mu(u, v)$, ...

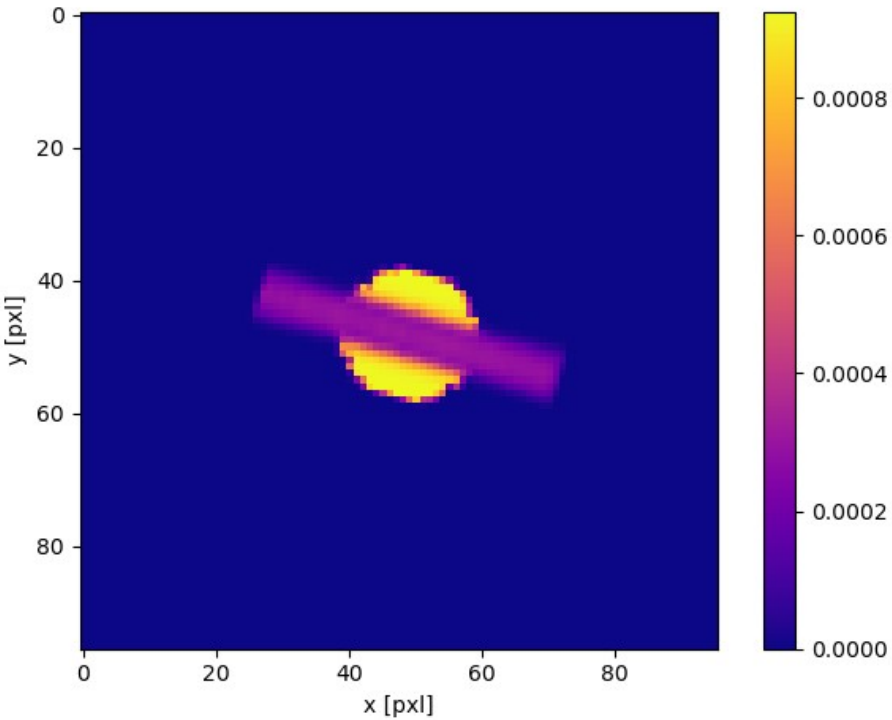

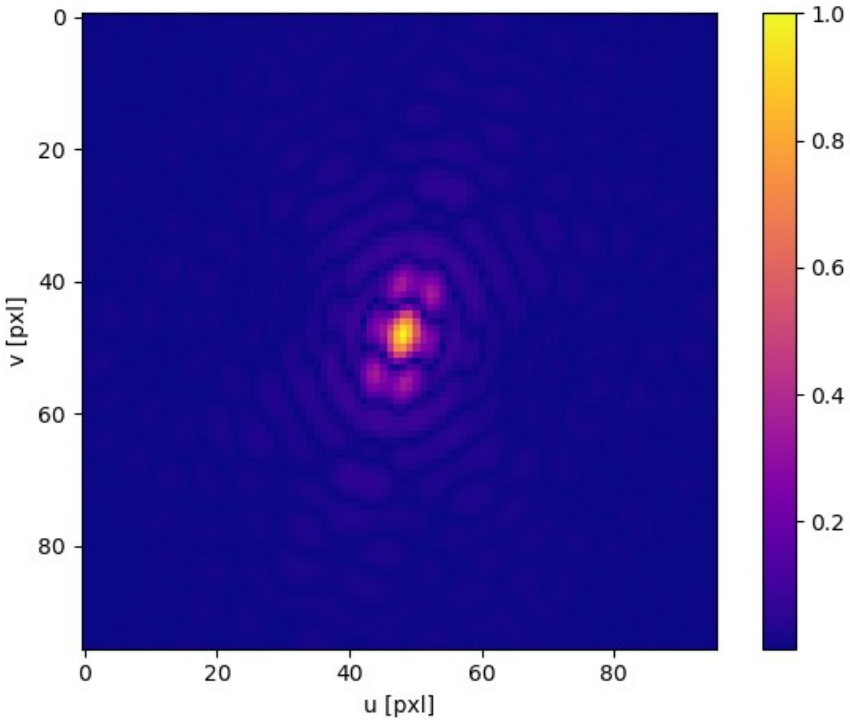

```
    ! linear limb-darkening coefficient at given lambda
    if (use_limbdark) then
      u_interp = interp(lambda_limb_(l-1), lambda_limb_(l), u_limb_(l-1,k), u_limb_(l,k), lambda)
    else
      u_interp = 0.d0
    endif

    if (debug_swift) then
      write(iuc,*) k, lambda, u_interp
    endif

    ! linear interpolation of integrated data to a given position in time
    xh_interp = interp(tout(j-1), tout(j), rh(j-1,k,1), rh(j,k,1), t_OBS(i))  ! k-th body, x coordinate
    yh_interp = interp(tout(j-1), tout(j), rh(j-1,k,2), rh(j,k,2), t_OBS(i))  ! y coordinate

    x = -xh_interp*AU / d  ! radians
    y = yh_interp*AU / d

    ! limb-darkened complex visibility (Hanbury-Brown et al. 1974)
    arg = pi_*phi(k)*B/lambda
    alpha = 1.d0-u_interp
    beta = u_interp

    mu = mu + Lum_lambda(k) * 1.d0/(alpha/2.0d0 + beta/3.d0) &
      * ( alpha*bessj1(arg)/arg + beta*sqrt(pi_/2.d0)*bessj32(arg)/arg**(3.d0/2.d0) ) &
      * exp(-2.d0*pi_*(0.d0,1.d0) * (u*x + v*y))

  endif
enddo  ! nbod

Vsq = (abs(mu)/Lumtot)**2
```

Brož et al. (2022, A&A 666, A24)

- HD 93206: Aa1, Aa2, Ac1, Ac2, Ab, Ad, B, C, D
- QZ Car: (Aa1+Aa2) + (Ac1+Ac2)
- data: SKY2, RV, TTV, SYN, SED, VIS, CLO, T3

- ESO archive: 098.D-0706(B), 099.D-0777(B)
- VLTI/GRAVITY pipeline (Freudling et al. 2013)
- $(u, v) \equiv \boldsymbol{B}/\lambda$ coverage, of wide orbit
- nominal vs. alternative models (~130-140 M_S)
- anomalous extinction? (R_V = 3.4, not 3.1)
- d = 2800 vs. 2450 pc

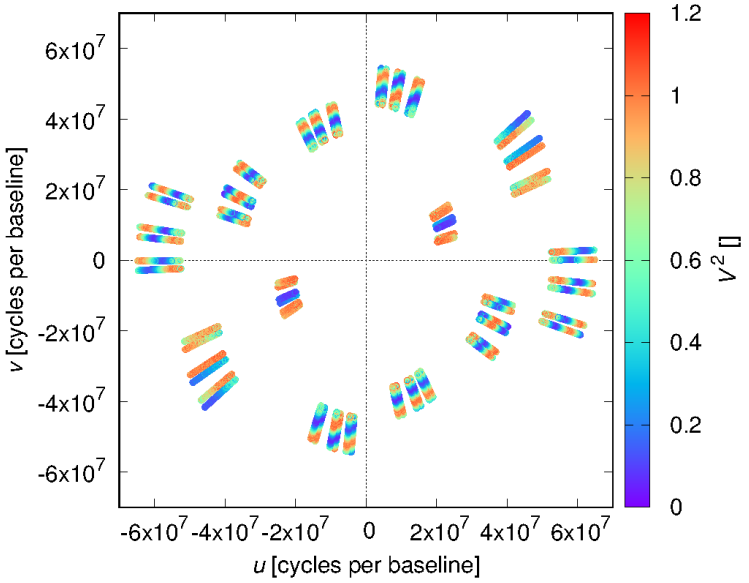

Fig. 3. Coverage $(u, v) \equiv \boldsymbol{B}/\lambda$ (in cycles per baseline) of new interferometric observations (see Table 1). The corresponding squared visibility V^2 is plotted in colour (see colour bar at right). The wide orbit ((Ac1+Ac2)+(Aa1+Aa2)), having the angular separation more than 30 mas, is clearly resolved.

VLTI

- high S/N, many λ, either precise astrometry (10 μas), or fitting of V^2, arg T_3

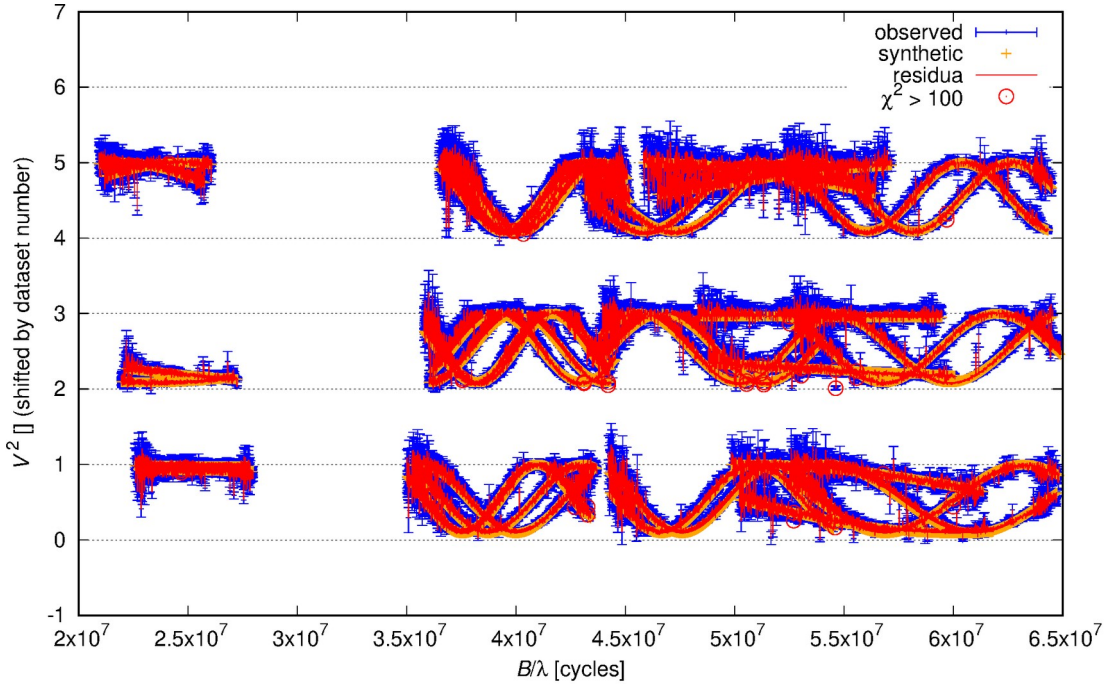

Fig. 12. Squared visibilities V^2 for VLTI/GRAVITY observations (March 14, 2017 and April 27, 2017; blue), synthetic V^2 (orange), and residuals (red). The sinusoidal dependence on the baseline B/λ essentially corresponds to a wide binary ((Ac1+Ac2)+(Aa1+Aa2)). Disks of individual stellar components cannot be resolved (at 0.08 mas, which correspond to a drop in V^2 of only 0.01 at the longest baseline).

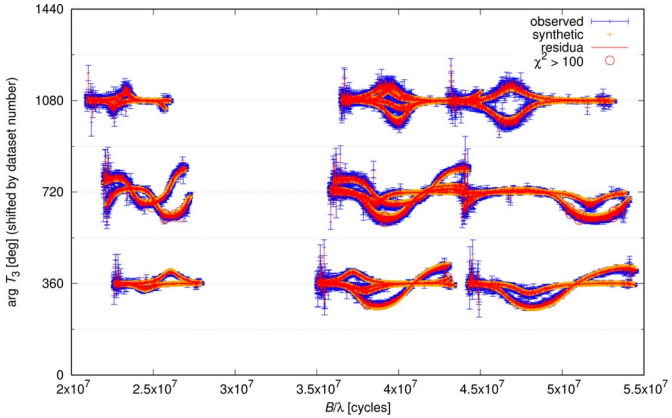

Fig. 13. Same as Fig. 12, but for the closure phase arg T_3. Again, the dependence on B/λ is similar to that of a binary.

best-fit models
convergence
parameters m_1 vs. m_2
contributions to χ^2
correlations
orthogonality

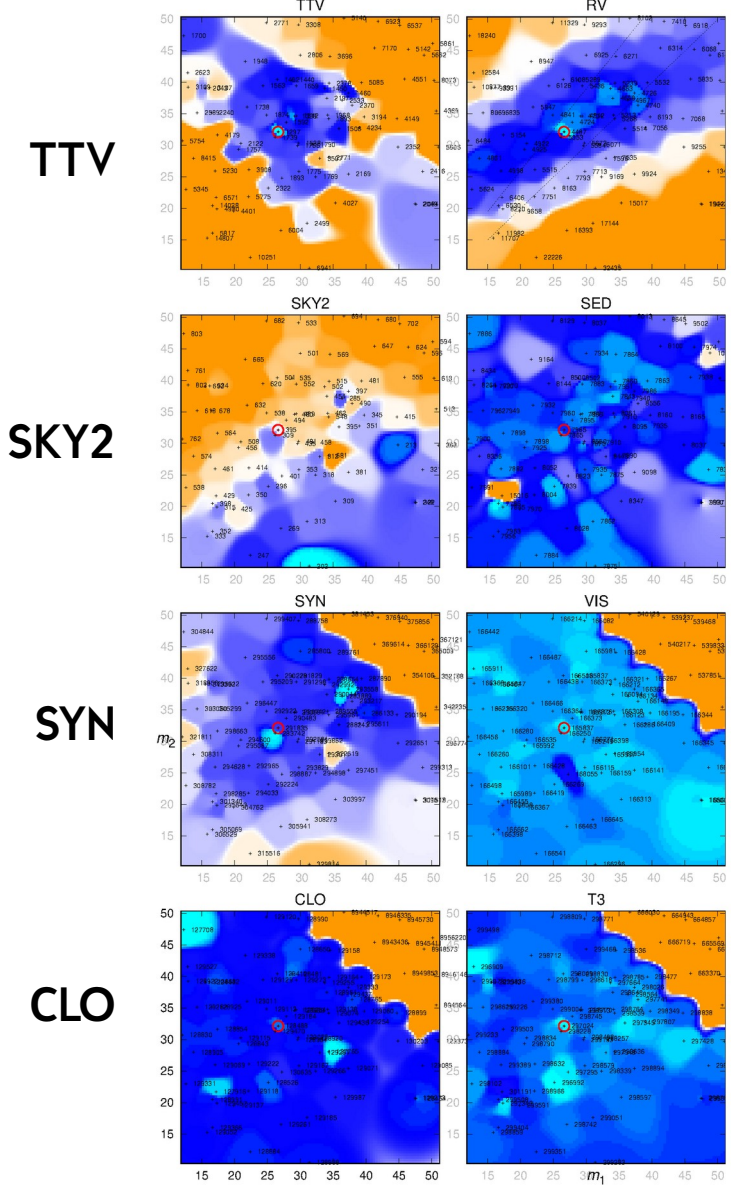

best fits
good fits
poor fits

Oplištilová et al. (2023, A&A 672, A31)

- HD 36486: Aa1, Aa2, Ab, B, Ca, Cb
- δ Ori A: (Aa1+Aa2) + Ab
- data: SKY, RV, TTV, ECL, SYN, SED, LC

- ESO archive: 078.D-0189(B)
- VLTI/AMBER interferometry
- AMDLIB pipeline (Tatulli et al. 2007)
- none corresponding to 1.3 mas?!
- see Oplištilová et al.

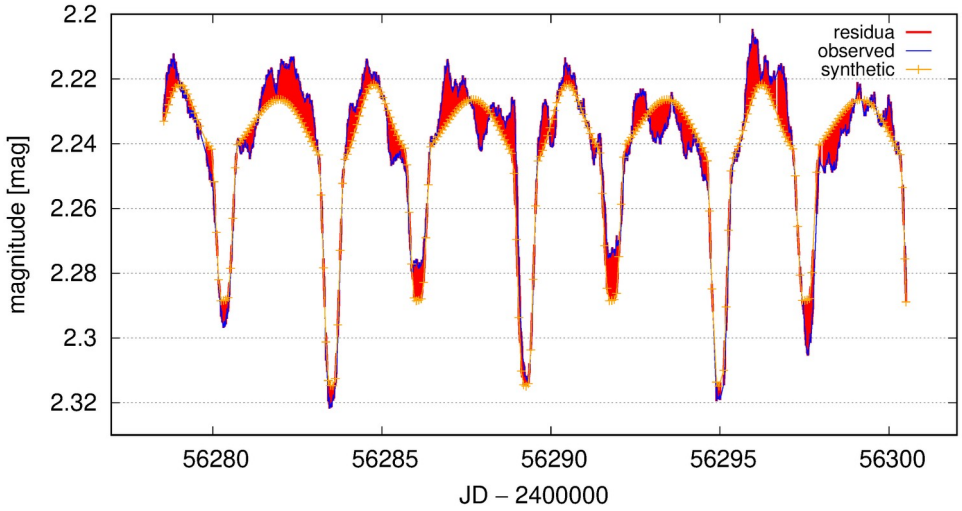

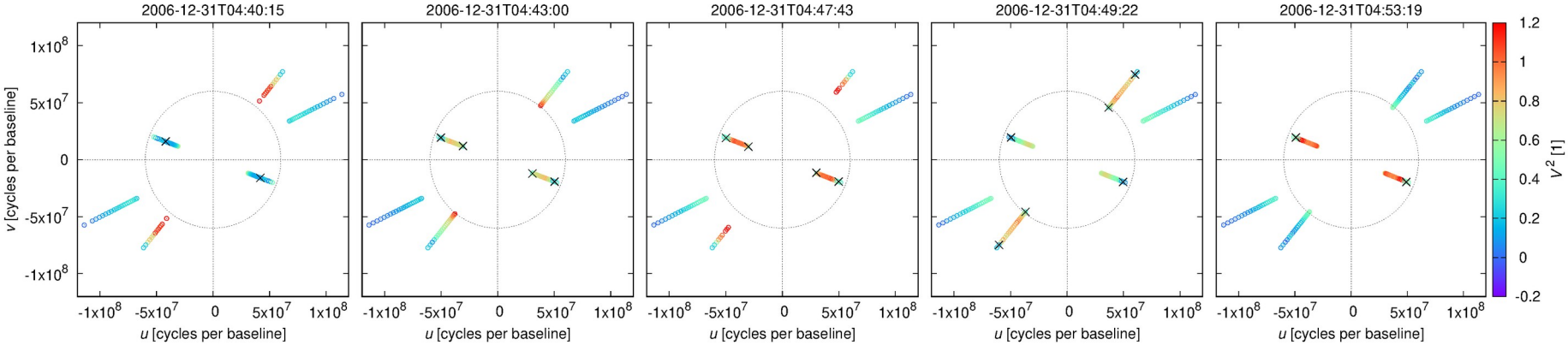

Fig. 21. Squared visibility V^2 vs. baselines $(u, v) \equiv \boldsymbol{B}/\lambda$ (in cycles per baseline) for δ Ori Aa1+Aa2 observed by the VLTI/AMBER. The observations are plotted as coloured points. The circle at 6×10^7 cycles is plotted for visual aid. V^2 is not perfectly stable; it should not change on the time scale of minutes. Sometimes, there is a 'drop' (low V^2; see black $\times$) at the beginning/end of the spectral bands (J, H, K). Consequently, we prefer observations with high V^2.

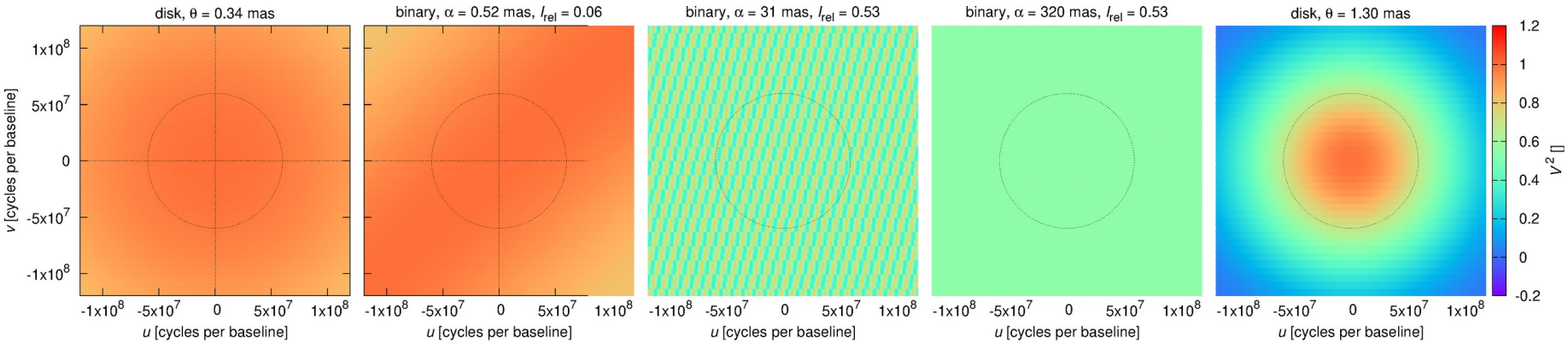

Fig. 22. Five analytical models of the squared visibility $V^2(u, v)$: a uniform disk ($\theta = 0.34$ mas), corresponding to the Aa1 component, a close binary ($\alpha = 0.52$ mas), corresponding to Aa1+Aa2, a wide binary ($\alpha = 31$ mas up to 320 mas), corresponding to (Aa1+Aa2)+Ab. None of these models fits the observations (Fig. 21). Alternatively, an extended disk ($\theta \simeq 1.30$ mas) may fit some of the observations. Possibly, it is related to a presence of circumbinary matter, encompassing the Aa1+Aa2 binary.

best-fit models
convergence
log g_1 vs. log g_3
contributions to χ^2
correlations
orthogonality

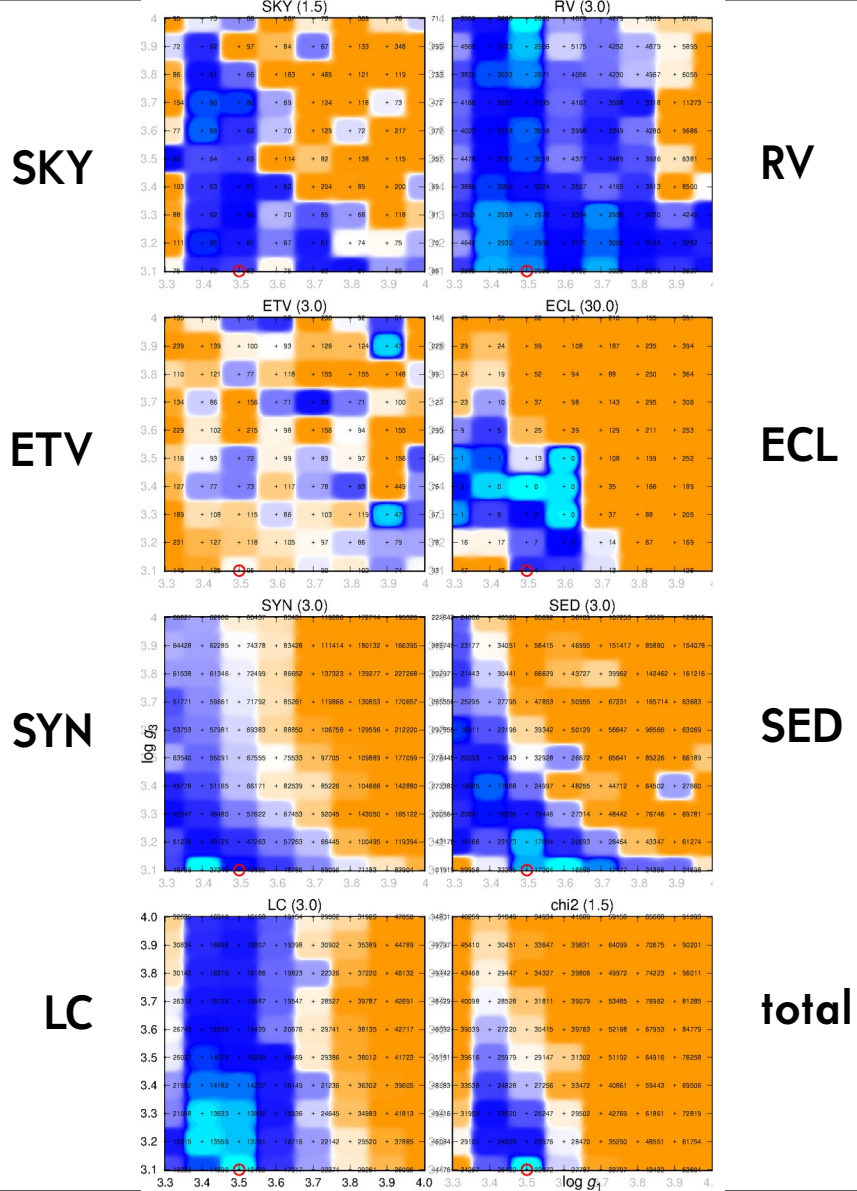

best fits
good fits
poor fits

Brož et al. (2021, A&A 653, A56)

- (216) Kleopatra + 2 satellites
- data: SKY, SKY2, SKY3, AO
- VLT/SPHERE/ZIMPOL, 3.6 mas/px
- deconvolution by MISTRAL (Fusco et al.)
- i.e., better than the diffraction limit of 8-m
- see also Marchis et al. (2021)

Brož et al. (2021, A&A 653, A56)

- (216) Kleopatra + 2 satellites
- data: SKY, SKY2, SKY3, AO
- VLT/SPHERE/ZIMPOL, 3.6 mas/px
- deconvolution by MISTRAL (Fusco et al.)
- i.e., better than the diffraction limit of 8-m
- see also Marchis et al. (2021)

Non-linearity of P_1, P_2

- cadence of observations (sparse)
- mutual perturbations of s.
- 1-d maps do *not* work
- local minima ← check them *all*[1]
- genetic algorithms do *not* work
- cf. stability!

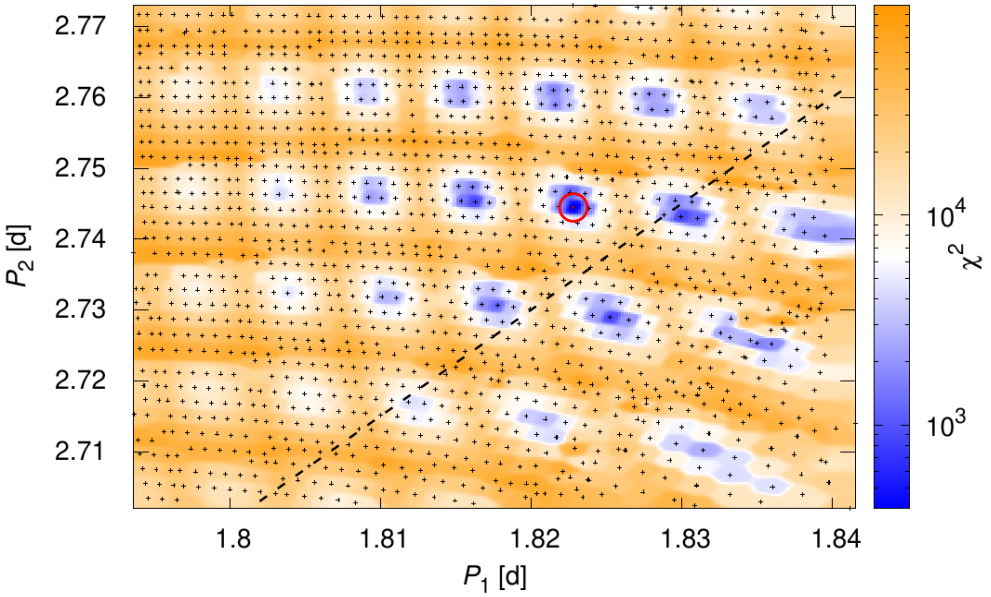

Fig. 4. $\chi^2 = \chi^2_{\rm sky}$ values for a range of periods P_1 and P_2 and optimised models. Every black cross denotes a local minimum (i.e. not a simple χ^2 map). All datasets (DESCAMPS, SPHERE2017, SPHERE2018) were used together, and consequently the spacing between local minima is very fine. The global minimum is denoted by a red circle. The dashed line indicates the exact 3:2 period ratio.

[1] i.e., 1 week on 100 CPUs

Model (Pyshellspec)

+ LTE level populations
+ LTE ionisation levels
+ 1D line-of-sight transfer
+ optically-thin (single) scattering ← no 3D, LI or ALI!
– non-isotropic scattering
+ prescribed ρ, T, v profiles
+ prescribed abundances
+ Voigt profile (prior to D.)
+ thermal broadening
+ microturbulence
+ natural
+ Stark
+ van der Waals
+ Doppler shift
+ HI bound-free continuum opacity
+ HI free-free
+ H^- bound-free,
+ H^- free-free

– Thomson scattering on free electrons
– Rayleigh scattering on neutral hydrogen
– Mie absorption on dust
– Mie scattering
– dust thermal emission
– line opacity
+ spherical primary (gainer)
+ Roche secondary (donor)
– black-body approximation (for *)
+ synthetic spectra (for *)
– irradiation
– reflection
+ limb darkening
+ gravity darkening
– heat transport

radiative transfer

$$I_\nu(0) = \int_0^{\tau_\nu} S_\nu \, \mathrm{e}^{-\tau'_\nu} \, \mathrm{d}\tau'_\nu + I^\star_\nu(\nu_2) f_{\mathrm{LD}} \, \mathrm{e}^{-\tau_\nu}$$

limb darkening

$$S_\nu = \frac{\epsilon_\nu}{\chi_\nu}$$

$$\nu_2 = \nu \left(1 - \frac{v^\star_z}{c}\right)$$

$$\chi_\nu = \kappa_\nu + \sigma_\nu$$

$$\kappa_\nu = \kappa_\nu^{\mathrm{line}} + \kappa_\nu^{\mathrm{odf}} + \kappa_\nu^{\mathrm{HIbf}} + \kappa_\nu^{\mathrm{HIff}} + \kappa_\nu^{\mathrm{H^-bf}} + \kappa_\nu^{\mathrm{H^-ff}}$$

$$\sigma_\nu = \sigma_\nu^{\mathrm{TS}} + \sigma_\nu^{\mathrm{RS}}$$

scattering

$$\epsilon_\nu = \epsilon_\nu^{\mathrm{th}} + \epsilon_\nu^{\mathrm{sc}}$$

$$\epsilon_\nu^{\mathrm{th}} = B_\nu(T(z))\kappa_\nu$$

$$\epsilon_\nu^{\mathrm{sc}} \doteq \sigma_\nu I^\star_\nu f_{\mathrm{SH}} \frac{\omega}{4\pi}$$

shadowing

geometrical constraints

$$H(R) = h_{\rm cnb}\sqrt{\frac{\gamma k_{\rm B} T}{\mu m_{\rm u}}}\frac{1}{\Omega_{\rm k}},$$

$$\Sigma(R) = \Sigma_{\rm nb}\left(\frac{R}{R_{\rm innb}}\right)^{e_{\rm densnb}},$$

$$\rho(R,0) = \frac{\Sigma}{\sqrt{2\pi}H},$$

$$\rho(R,z) = \rho(R,0)\exp\left[-\min\left(\frac{z^2}{2H^2};\frac{h_{\rm windnb}^2}{2}\right)\right],$$

$$T(R,0) = T_{\rm nb}\left(\frac{R}{R_{\rm innb}}\right)^{e_{\rm tmpnb}},$$

$$T(R,z) = T(R,0)\max\left(1;1+(t_{\rm invnb}-1)\frac{|z|-h_{\rm invnb}H}{a_{\rm neb}H-h_{\rm invnb}H}\right),$$

$$v_r(R) = \mathcal{H}(|z|-h_{\rm velnb}H)\,v_{\rm nb}\left(1-\frac{R_{\rm innb}}{R}\right)^{e_{\rm velnb}},$$

$$v_\phi(R) = \sqrt{\frac{GM_\star}{R}},$$

$$\rho(R) = \rho_{\rm jt}\left(\frac{R_{\rm injt}}{R}\right)^2\frac{v_r(R_{\rm injt})}{v_r(R)}\,(1\pm a_{\rm symjt}),$$

$$T(R) = T_{\rm jt}\left(\frac{R}{R_{\rm injt}}\right)^{e_{\rm tmpjt}},$$

$$v_r(R) = v_{\rm jt}\left(1-\frac{R_{\rm cjt}}{R}\right)^{e_{\rm veljt}},$$

$$\rho(R) = \rho_{\rm sh}\left(\frac{R_{\rm insh}}{R}\right)^2\frac{v_r(R_{\rm insh})}{v_r(R)},$$

$$T(R) = T_{\rm sh}\left(\frac{R}{R_{\rm insh}}\right)^{e_{\rm tmpsh}},$$

$$v_r(R) = v_{\rm sh}\left(1-\frac{R_{\rm csh}}{R}\right)^{e_{\rm velsh}}.$$

χ^2 terms

$$\chi^2 = \chi^2_{\rm lc} + \chi^2_{\rm vis} + \chi^2_{\rm clo} + \chi^2_{\rm t3} + \chi^2_{\rm sed} + \chi^2_{\rm spe} + \chi^2_{\rm vamp} + \chi^2_{\rm vphi},$$

$$\chi^2_{\rm lc} = \sum_{k=1}^{N_{\rm band}} \sum_{i=1}^{N_{{\rm lc}\,k}} \left(\frac{m_{ki}^{\rm obs} - m_{ki}^{\rm syn}}{\sigma_{ki}} \right)^2,$$

$$\chi^2_{\rm vis} = \sum_{i=1}^{N_{\rm vis}} \left(\frac{|V_i^{\rm obs}|^2 - |V_i^{\rm syn}|^2}{\sigma_i} \right)^2,$$

$$\chi^2_{\rm clo} = \sum_{i=1}^{N_{\rm clo}} \left(\frac{\arg T_{3i}^{\rm obs} - \arg T_{3i}^{\rm syn}}{\sigma_i} \right)^2,$$

$$\chi^2_{\rm t3} = \sum_{i=1}^{N_{\rm clo}} \left(\frac{|T_{3i}|^{\rm obs} - |T_{3i}|^{\rm syn}}{\sigma_i} \right)^2,$$

$$\chi^2_{\rm sed} = \sum_{i=1}^{N_{\rm sed}} \left(\frac{F_{\lambda i}^{\rm obs} - F_{\lambda i}^{\rm syn}}{\sigma_i} \right)^2,$$

$$\chi^2_{\rm spe} = \sum_{i=1}^{N_{\rm spe}} \left(\frac{I_{\lambda i}^{\rm obs} - I_{\lambda i}^{\rm syn}}{\sigma_i} \right)^2,$$

$$\chi^2_{\rm vamp} = \sum_{k=1}^{N_{\rm set}} \sum_{i=1}^{N_{{\rm vamp}\,k}} \left(\frac{V_i^{\rm obs} - V_i^{\rm syn} f_k}{\sigma_i} \right)^2,$$

$$\chi^2_{\rm vphi} = \sum_{k=1}^{N_{\rm set}} \sum_{i=1}^{N_{{\rm vphi}\,k}} \left(\frac{\arg V_i^{\rm obs} - \arg V_i^{\rm syn} + g_k + h_k}{\sigma_i} \right)^2,$$

factors

offsets & slips

Model (cont.)

- http://sirrah.troja.mff.cuni.cz/~mira/betalyr/
- Shellspec + Python = Pyshellspec (J. Budaj, J. Nemravová)
- calculation of interferometric observables (DFT), of χ^2
- multiprocessing module (split along λ; 4-16 cores)
- discretisation $N_x = 160$, $N_y = 60$ (~1 $R_\odot$); variable in z (~τ)
- local & global optimisation (simplex, differential evolution, ...)
- 1 iteration: 2392 synthetic images (3 min)
- 1 convergence: >10^3 steps (1 week)
- free parameters: i, Ω, d, T_{cp}, T_{nb}, T_{invnb}, ϱ_{nb}, R_{innb}, R_{outnb}, h_{invnb}, h_{windnb}, h_{cnb}, h_{shdnb}, v_{nb}, v_{trbnb}, e_{dennb}, e_{tmpnb}, e_{velnb}, etc. other objects, ...
- fixed parameters: P, $a \sin i$, e, ω, γ, JD_{min}, M_1, $q = M_1/M_2$, f_{ill}, R_{star}, T_{star}, d_{cp}, h_{velnb}, ...

convergence
(simplex)

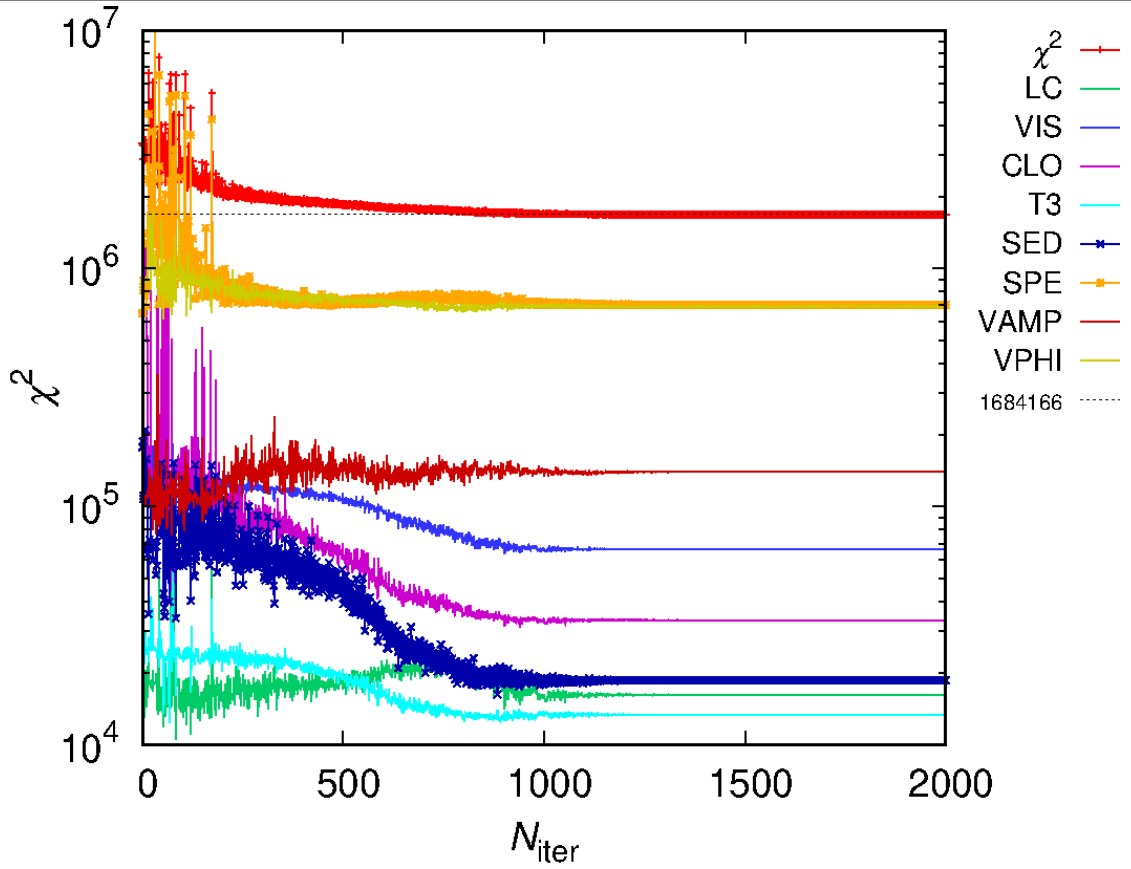

Fig. 6. χ^2 convergence (red) for joint model; individual contributions (LC, VIS, CLO, T3, SED, SPE, VAMP, VPHI) are also indicated. The model successfully converges to a local minimum. Some datasets have a substantially larger number of observations, (i.e. effectively a larger weight). The χ^2 values are different from Table 1 because the model was re-converged several times, and uncertainties of some datasets were modified.

Continuum images

- NUV → FIR, optically thick

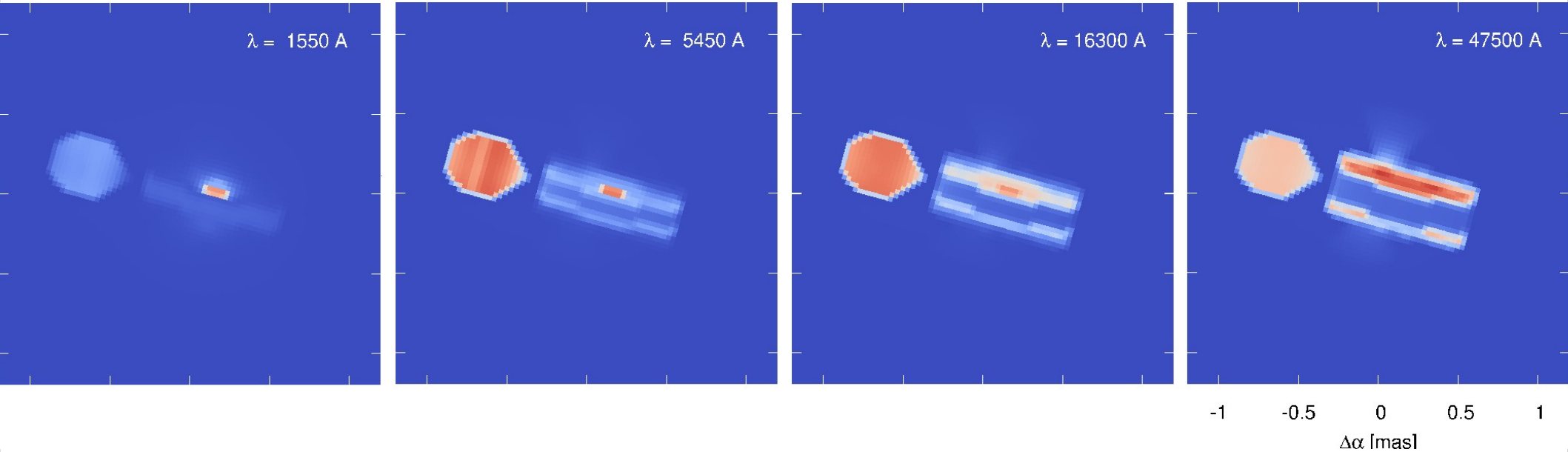

Line images

- Hα, optically thin

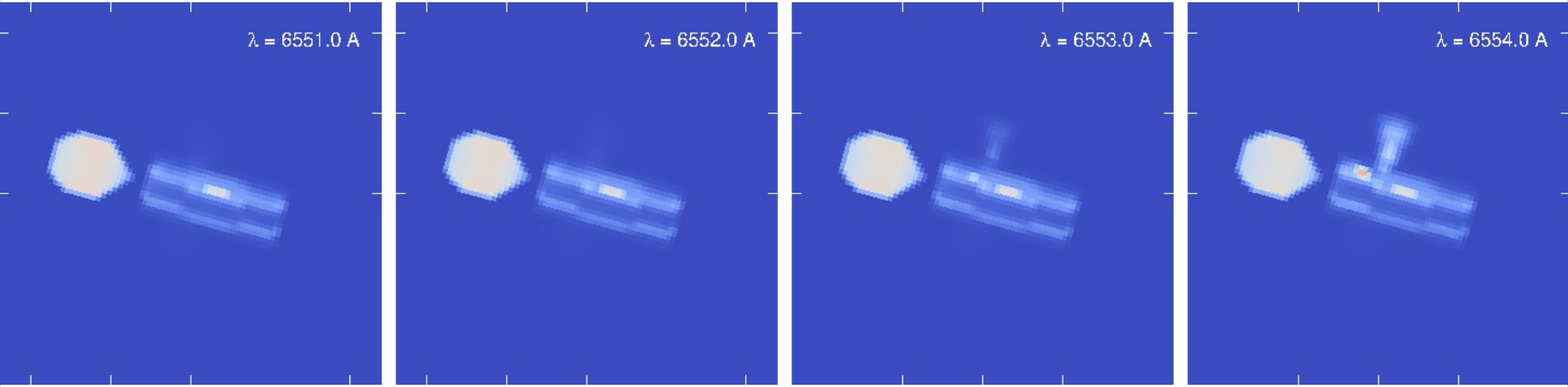

Line images

- Hα, optically thin

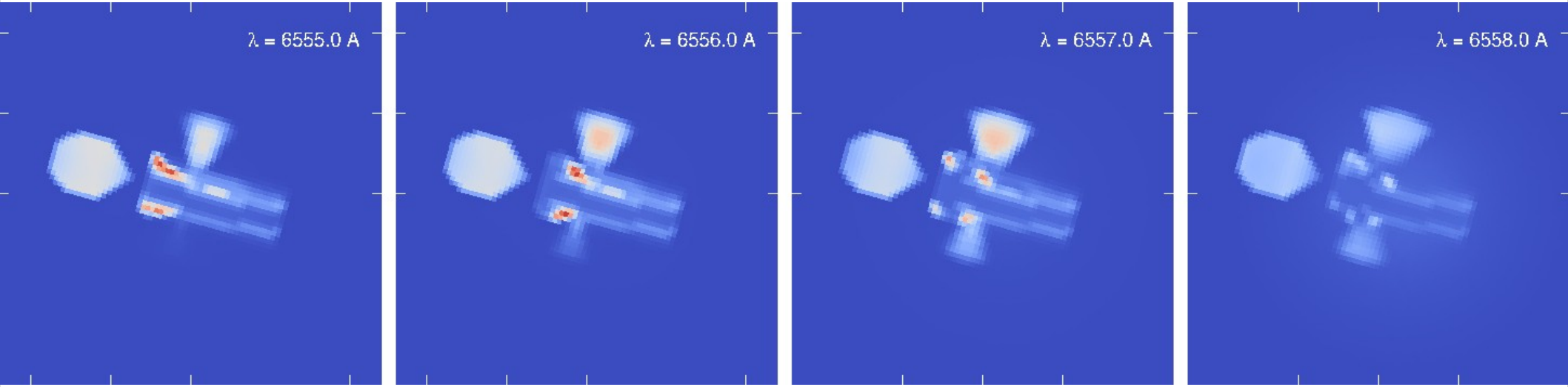

Line images

- Hα, optically thin

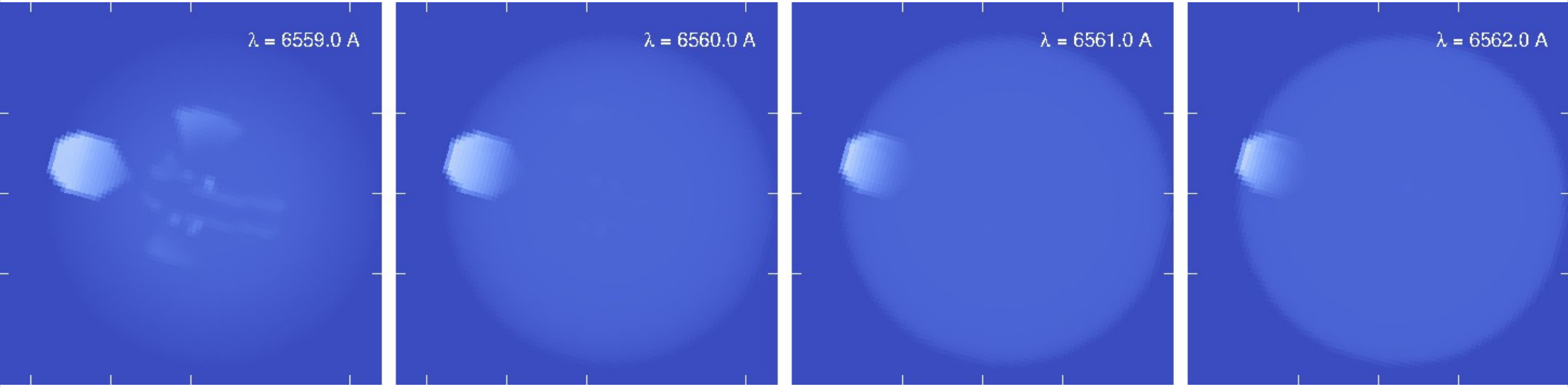

Line images

- Hα, optically thin

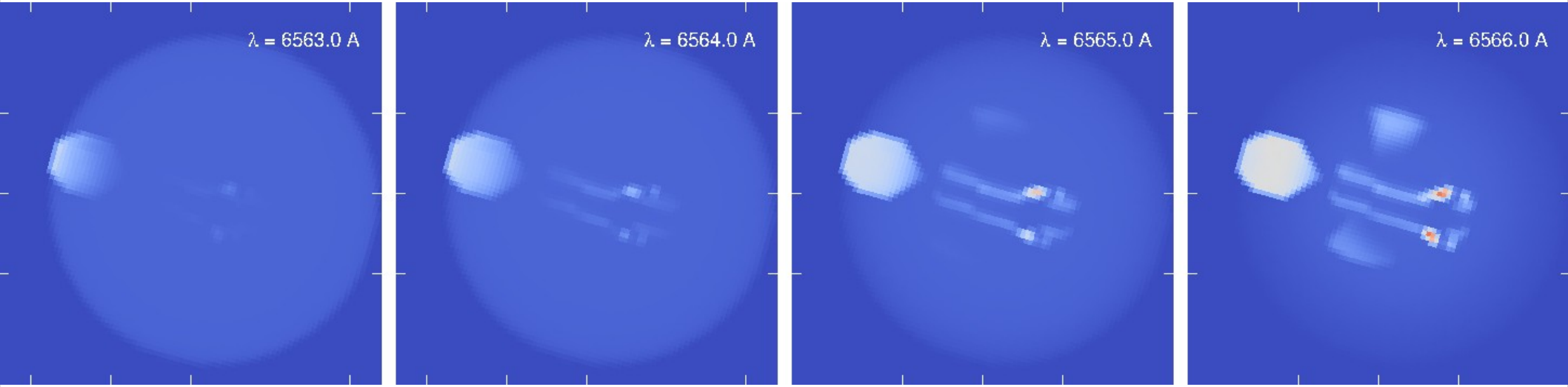

Line images

- Hα, optically thin

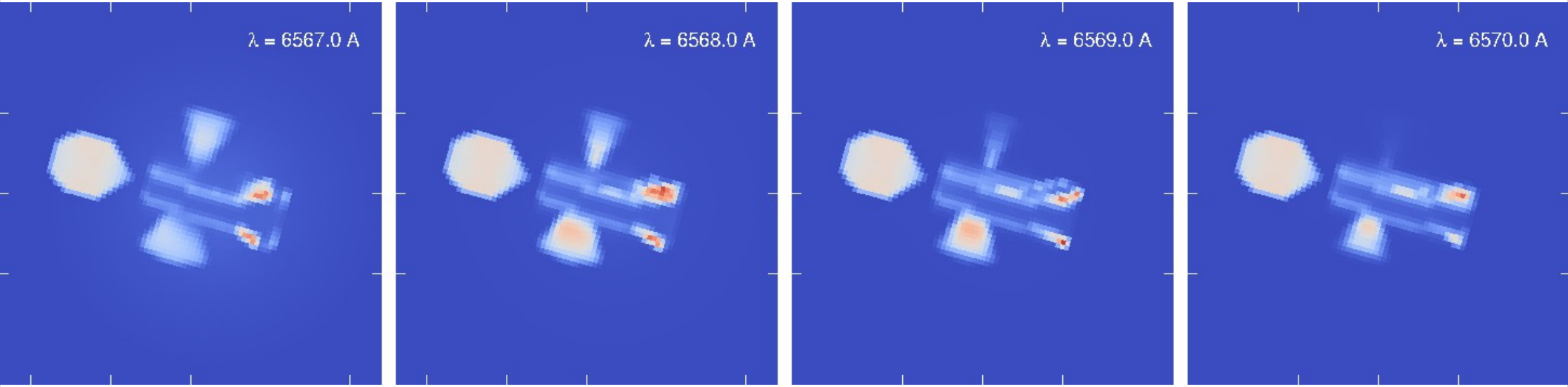

Line images

- Hα, optically thin

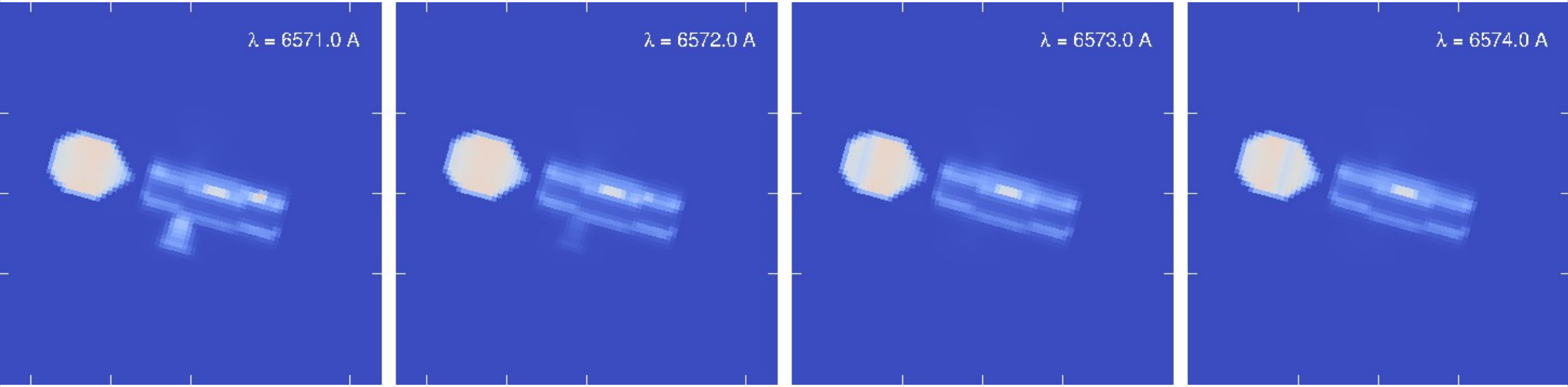

Observation-specific model(s)

- a ‘tension’ between datasets, cf. unconstrained parameters, cf. limits of p.

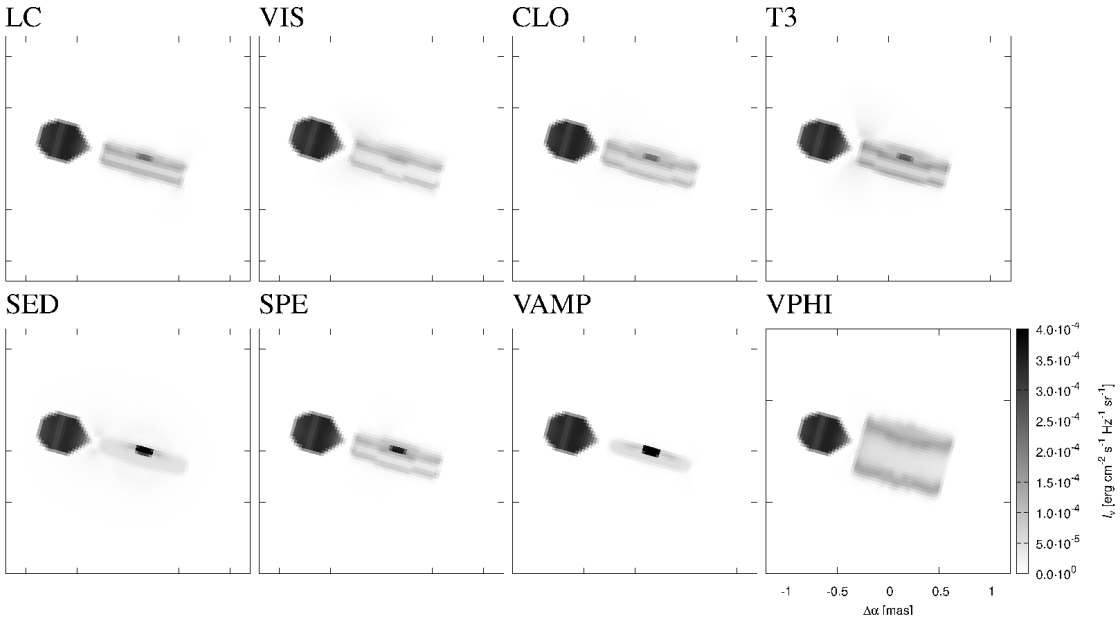

Fig. 18. Continuum synthetic images for observation-specific models (datasets LC, VIS, CLO, T3, SED, SPE, VAMP, and VPHI) for the wavelength 545 nm (V). The apparent differences (e.g. the thickness of the disc, the appearance of the primary) demonstrate systematics between datasets. Alternately, some datasets (e.g. VPHI) do not constrain certain parameters.

squared visibility

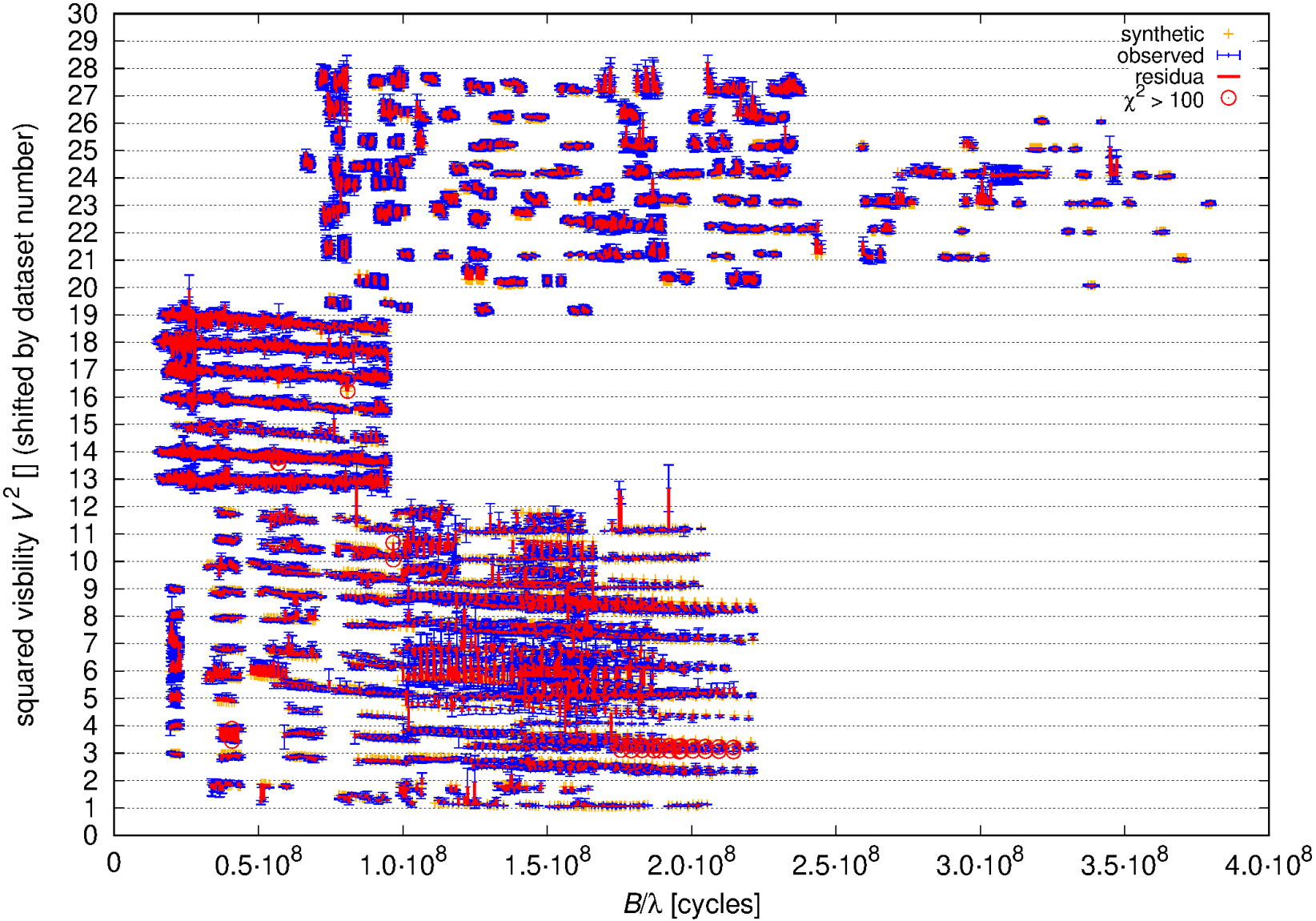

Differential visibility

- if visibility decreases (across Hα) → size must increase...

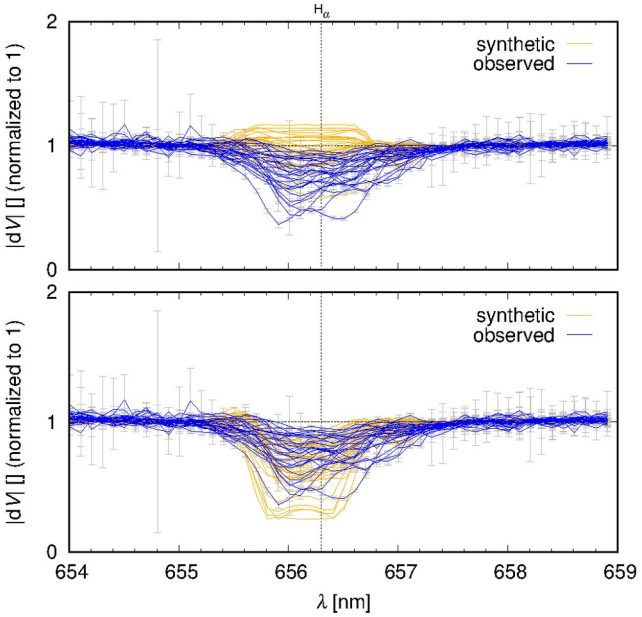

Fig. 5. Observed differential visibility amplitude $|dV|$ versus wavelength λ, normalised to 1 in the continuum (blue), and its decrease across the Hα profile. Uncertainties of $|dV|$ are also plotted (grey). Synthetic visibilities (yellow) are shown for the two "extreme" values of the shell's outer radius $R_{outsh} = 40\,R_\odot$ (*top*) and $120\,R_\odot$ (*bottom*).

Chemical composition

- if Hα is in emission → CII must be in emission...

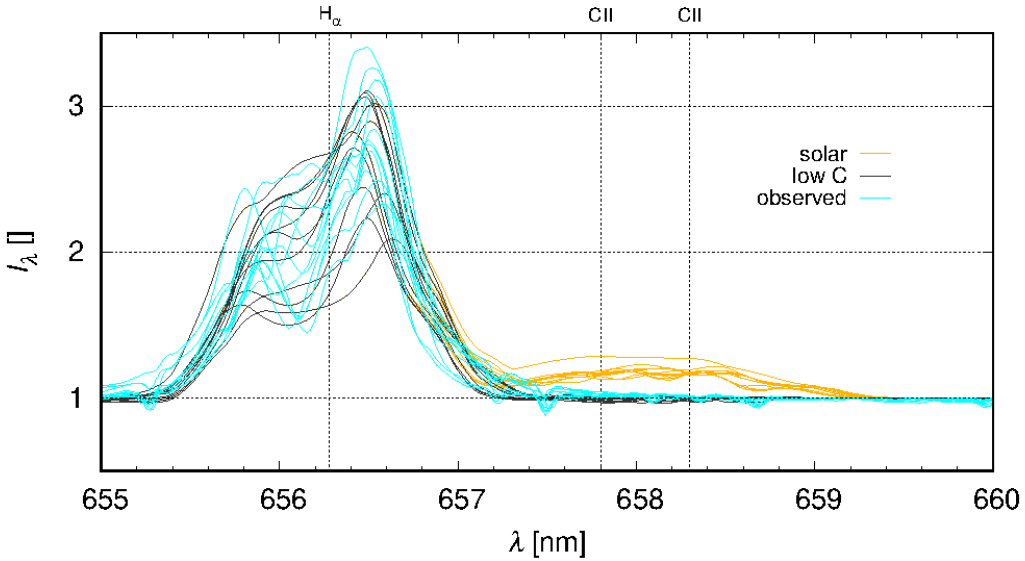

Fig. 20. Synthetic spectra for solar abundances (yellow) and 10^{-2} lower abundance of C (grey); observed spectra (blue) are plotted for comparison. For the solar composition, C II 6578 and 6583 emission is too strong.

Vitovský (in prep.)

- analytical accretion disk of Shakura & Sunyæv (1973), w. viscosity $\nu = \alpha c_s H$
- modified for a *general* opacity prescription $\kappa = \kappa_0 \rho^A T^B$
- constrained by the accretion rate of β Lyr A, $dM/dt = 2 \cdot 10^{-5}\ M_S\ y^{-1}$
- radial profiles $\Sigma(r)$, $T(r)$, $H(r)$ compared to "observations" (Brož et al. 2021)

- most models excluded due to self-consistency (P_{gas} vs. P_{rad}); κ is Kramers
- Σ must be much higher! 10000 kg m^{-2} at the inner rim, if $\alpha = 0.1$
- T must be much higher! 10^5 K in the mid-plane
- cf. vertical scale height H *is* hydrostatic (low μ)
- steep vertical gradient & inversion in disk atmosphere?

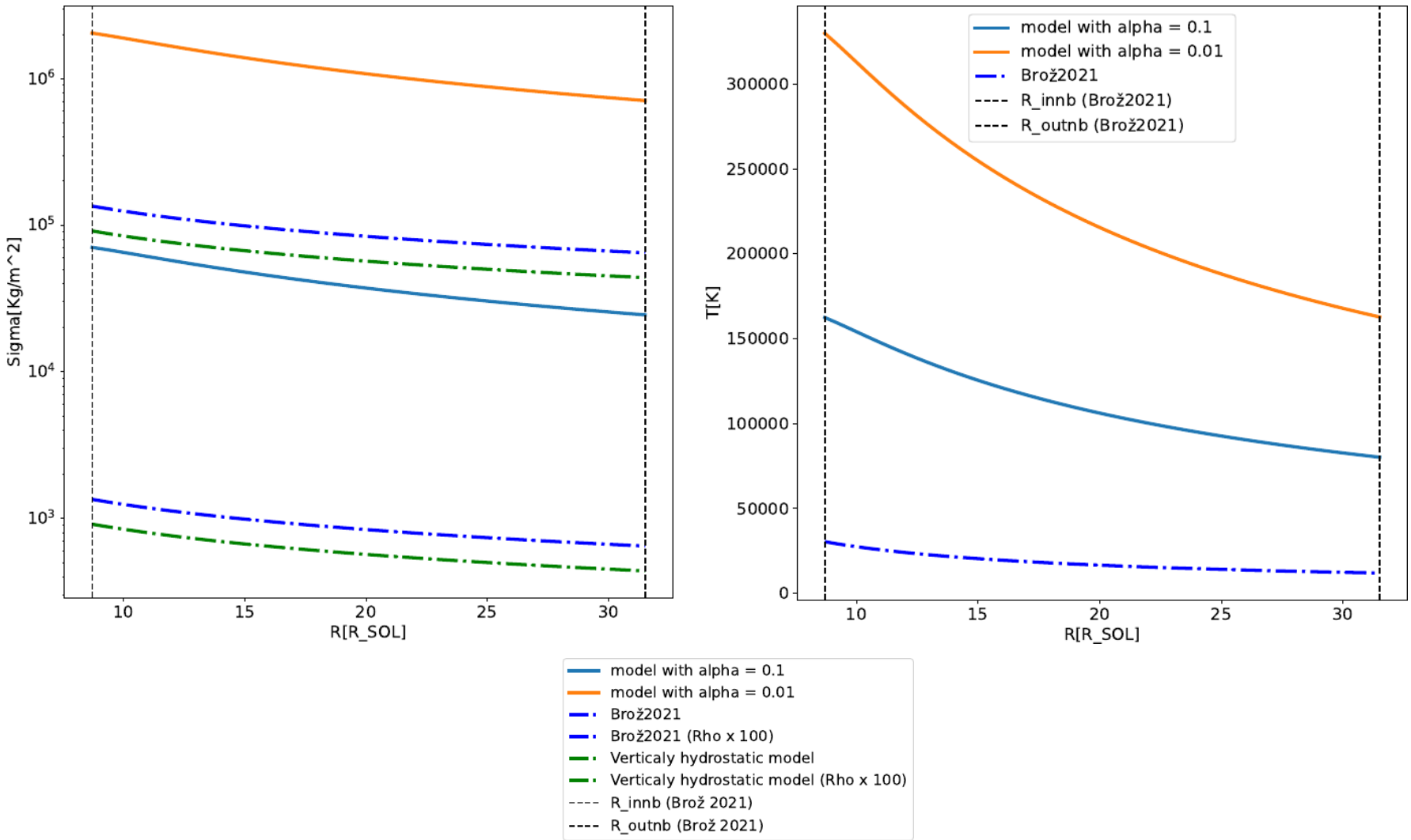
Sigma[Kg/m^2]
10^6
10^5
10^4
10^3
10
15
20
25
30
R[R_SOL]
T[K]
300000
250000
200000
150000
100000
50000
0
model with alpha = 0.1
model with alpha = 0.01
Brož2021
R_innb (Brož2021)
R_outnb (Brož2021)
model with alpha = 0.1
model with alpha = 0.01
Brož2021
Brož2021 (Rho x 100)
Verticaly hydrostatic model
Verticaly hydrostatic model (Rho x 100)
R_innb (Brož 2021)
R_outnb (Brož 2021)

Caveats

- Is (u, v) coverage sufficient? "1 visibility ~ 1 pixel"
- Is a * resolved or not? (cf. Airy)
- Is a * in the aperture?
- What is the *state* of instrument?
- Is a model sufficient?
- Is a model resolution-dependent?
- Adding an optically-thin object changes other objects!
- Some parameters seem to be more important than expected (e.g., v_{turb}, Z).
- A 'tension' between individual datasets (LC, VIS, CLO, T3, SED, SPE, VAMP, VPHI)?
- Not-so-successful models are useful to exclude...

Brož et al. (2023, A&A 676, A60)

- (22) Kalliope + 1 satellite
- data: SKY, AO, LC2, OCC
- occultations, transits, eclipses (20 mmag)
- TRAPPIST, SPECULOOS (3-5 mmag)
- see also Ferrais et al. (2022)

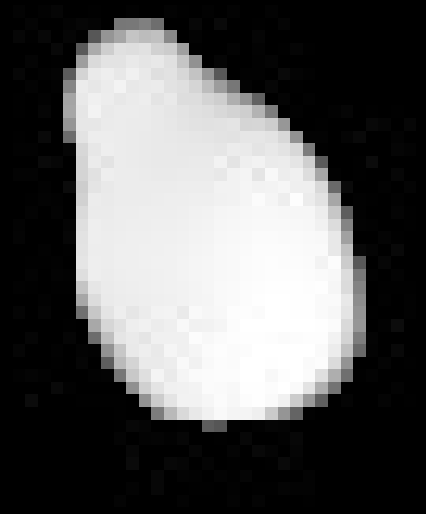

Brož et al. (2023, A&A 676, A60)

- (22) Kalliope + 1 satellite
- data: SKY, AO, LC2, OCC
- occultations, transits, eclipses (20 mmag)
- TRAPPIST, SPECULOOS (3-5 mmag)
- see also Ferrais et al. (2022)

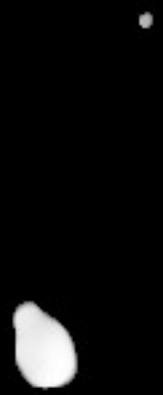

Correlation of P and C_{20}

- high $|C_{20}|$ → precession rate $d\Omega/dt$ → low P
- cf. local minima; P must be preset!
- 2 or 3 precession cycles
- a preferred solution $C_{20} = -0.20$, i.e., differentiated oblate interior?
- a homogeneous body excluded!

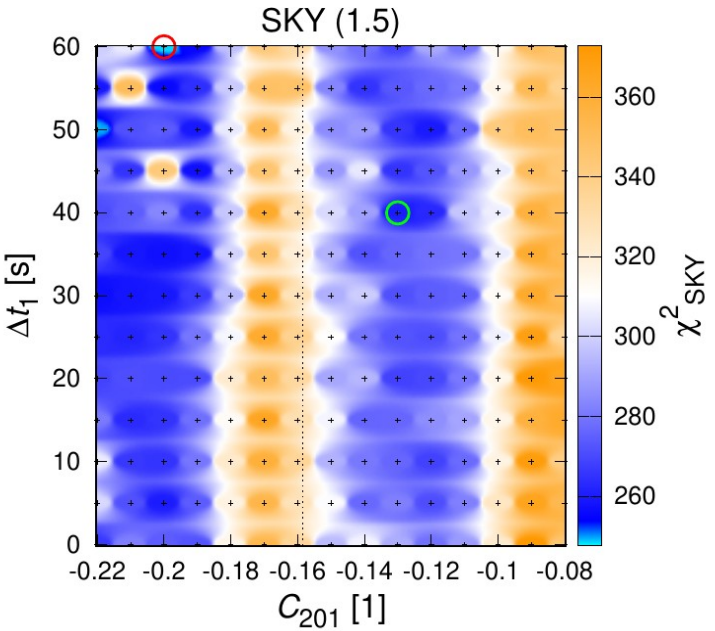

Fig. 12. Quadrupole moment $C_{20,1}$ vs. the tidal time lag Δt_1 of the central body. The corresponding $\chi^2_{\rm sky}$ values are plotted as colours (cyan, blue, white, and orange) and as numbers (gray). SKY and AO datasets were used. Models were converged for 195 combinations of the fixed parameters; all other parameters were free. For each combination, 1000 iterations were computed, that is, 195 000 models in total. Homogeneous body with $C_{20,1} = -0.1586$ is excluded. Preferred solutions are either $\simeq -0.20$, or $\simeq -0.12$, indicated by red and green circles.

Polygonal algorithm

1st clipping:
partial shadowing
back-projection
2nd clipping:
partial visibility
back-projection
'killed' d. errors

Vatti (1992)
Prša et al. (2016)
Clipper2 C++ library

structures[1]
optimisations[2]

[1] set of sets of polygons
[2] bounding-box tests

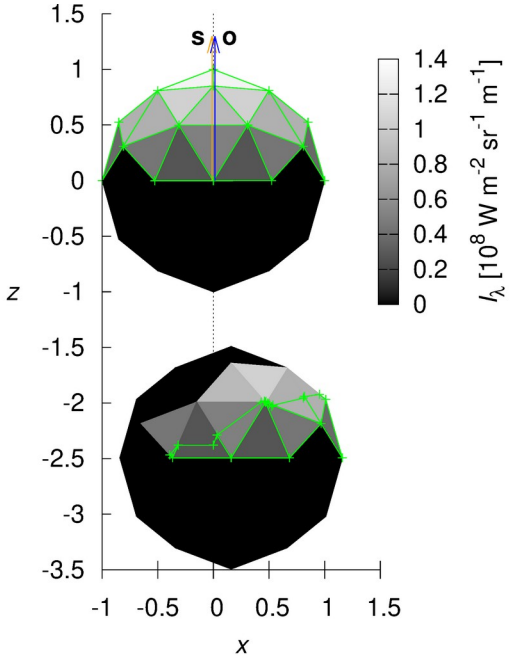

Fig. 1. Two-sphere test of the polygon light curve algorithm. We can even use a very coarse discretisation of 42 nodes for each sphere, because we compute partial eclipses, partial occultations, or partial transits. Shades of gray show the monochromatic intensity I_λ (in W m^{-2} sr^{-1} m^{-1}), green lines show the non-eclipsed and non-occulted polygons used to compute the surface areas. The orange arrow shows the direction towards the Sun and blue towards the observer. The test bodies are metre-sized, 1 au from the Sun and 1 au from the observer. See also Fig. 2.

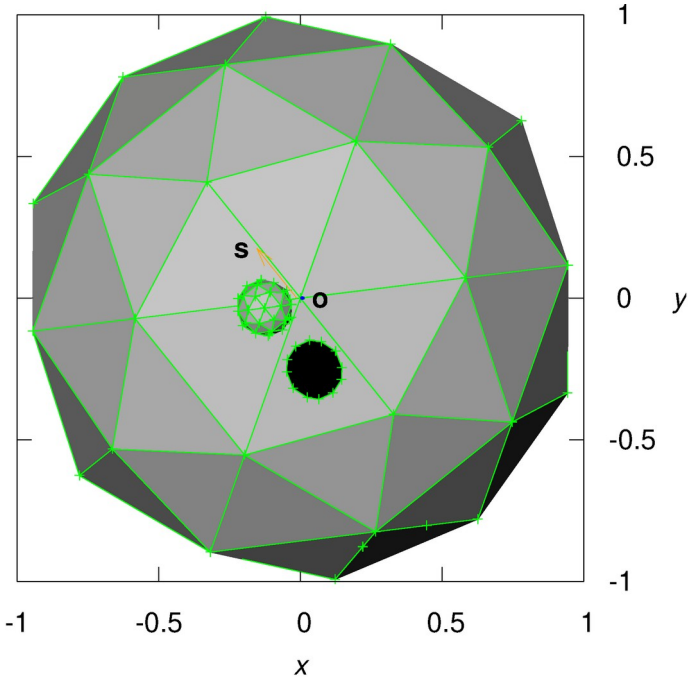

Fig. 3. Similar to Fig. 1. A tiny-triangle test, where one body is large and other body is small. It demonstrates that annular eclipses, as well as partial eclipses, partial occultations, and partial transits, are computed exactly. The polygon corresponding to the shadow (black) has a negative signed area.

```fortran
! Notation:
!
! c .. count
! s .. set of polygons
! p .. polygon
!
! size(polys1)           .. count of sets
! polys1(1)%c            .. count of polygons
! polys1(1)%s(1)%c       .. count of nodes
! polys1(1)%s(1)         .. 1st polygon in a set
! polys1(1)%s(1)%p(1,:) .. 1st node in a polygon
! polys1(1)%s(1)%p(1,1) .. 1st node, x-coordinate

module polytype_module

use iso_c_binding

include 'polytype.inc'

type, bind(c) :: polytype
  integer(c_int) :: c = 0
  real(c_double), dimension(MAXPOLY,3) :: p
end type polytype

type, bind(c) :: polystype
  integer(c_int) :: c = 0
  type(polytype), dimension(MAXPOLYS) :: s
end type polystype

end module polytype_module
```

```fortran
call boundingbox(polys2, boxes)

polys3(:)%c = 0

!$omp parallel do private(i,j,poly_i,poly_j,poly_k) shared(polys2,polys3,boxes)
do i = 1, size(polys2,1)
  if (polys2(i)%c.eq.0) cycle
  poly_i = polys2(i)
  c = 0

  do j = 1, size(polys2,1)
    if (j.eq.i) cycle                                                  ! self-shadowing
    if (poly_i%c.eq.0) exit                                            ! no-polygons-in-set
    if (polys2(j)%c.eq.0) cycle                                        ! no-points-in-polygon
    if ((boxes(j,2).lt.boxes(i,1)).or.(boxes(j,1).gt.boxes(i,2))) cycle  ! bounding-box-in-u
    if ((boxes(j,4).lt.boxes(i,3)).or.(boxes(j,3).gt.boxes(i,4))) cycle  ! bounding-box-in-v
    if (boxes(j,6).lt.boxes(i,6)+EPS) cycle                            ! is-in-front

    call clip_in_c(poly_i, polys2(j), poly_k)

    c = c+1

    include 'c1.inc'
  enddo

  polys3(i) = poly_i
  clips(i) = clips(i)+c
enddo
!$omp end parallel do

deallocate(boxes)
```

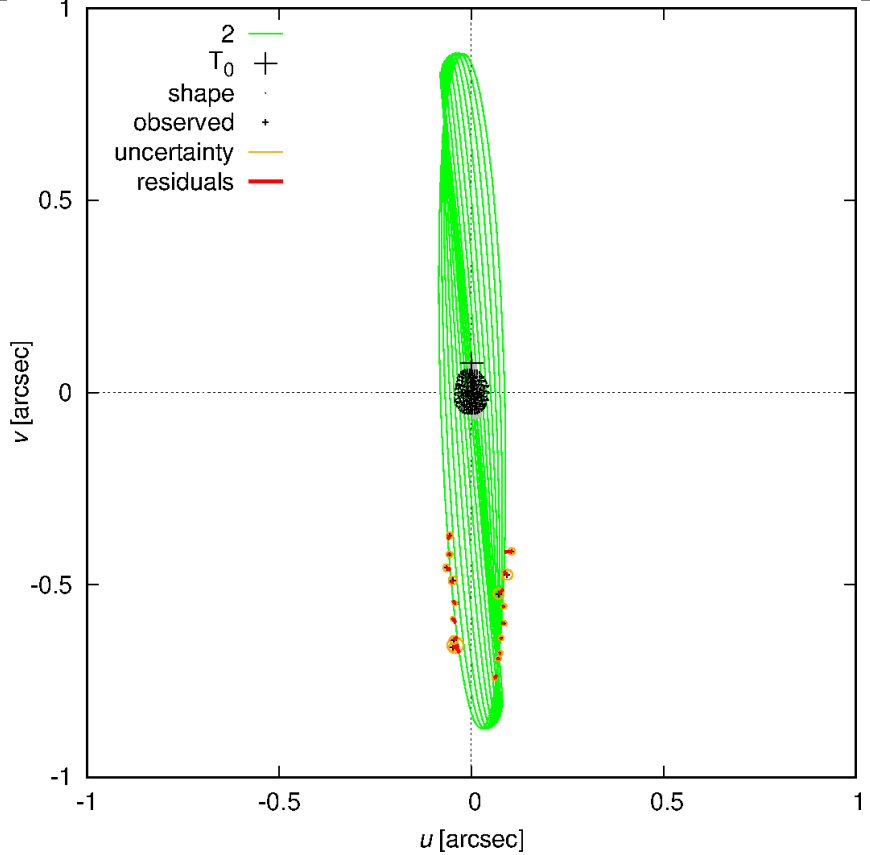

Fig. 9. Orbit of Linus in the (u, v) plane, derived from the short-arc astrometric + photometric model. It fits the PISCO dataset around 2459579, namely, close to the mutual occultation events, when the orbit is seen from the edge. The synthetic orbit of Linus (i.e., body 2) is plotted in green, the observed astrometry in yellow, the residuals in red, the shape of (22) in black. The viewing geometry is changing in the course of time; otherwise the orbit is elliptical. The position at the reference epoch T_0 is marked by the cross. The contribution to χ^2 is $\chi^2_{\rm sky}$ = 27 and $n_{\rm sky}$ = 36.

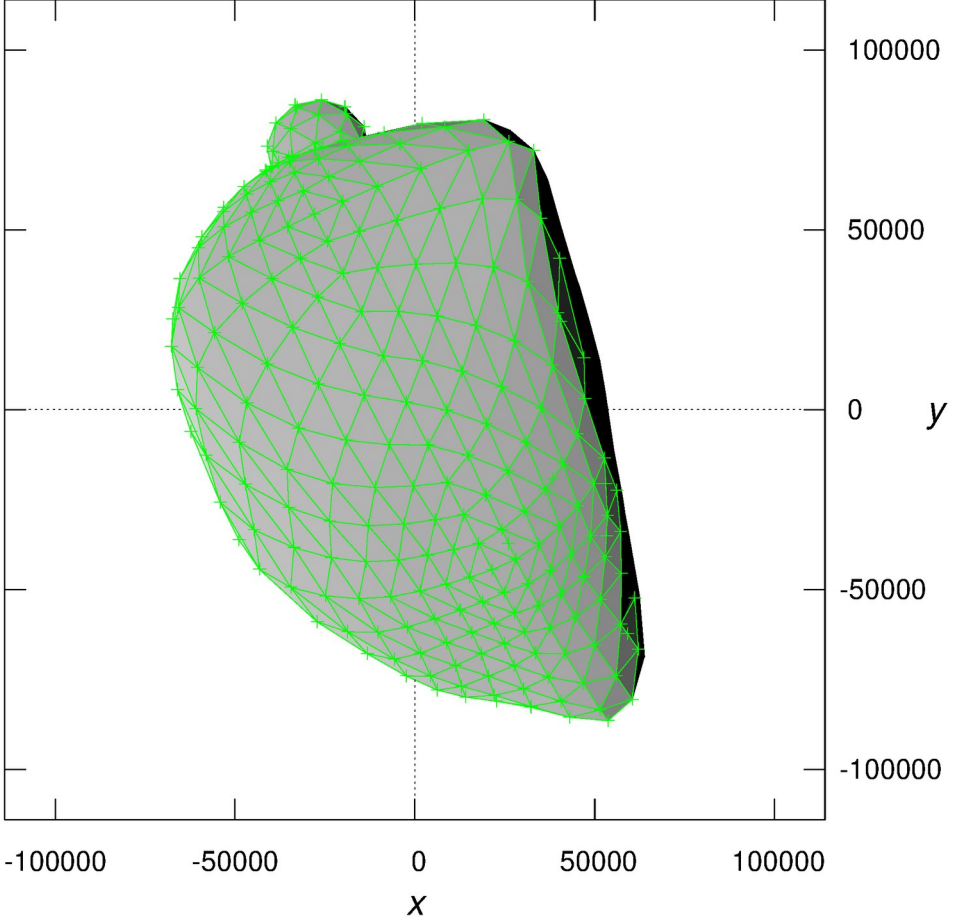

Fig. 11. Example of geometry for the mutual occultation of Linus by (22) Kalliope, namely, the event 2459546. The monochromatic intensity I_λ (in $\mathrm{W\,m^{-2}\,sr^{-1}\,m^{-1}}$) is shown as shades of gray. The ADAM shape model with 800 faces was used for (22), and a sphere with 80 faces for Linus. It is sufficient because partial occultations of faces were computed by the polygonal light curve algorithm.

exact light curve
scattered light
Hapke law

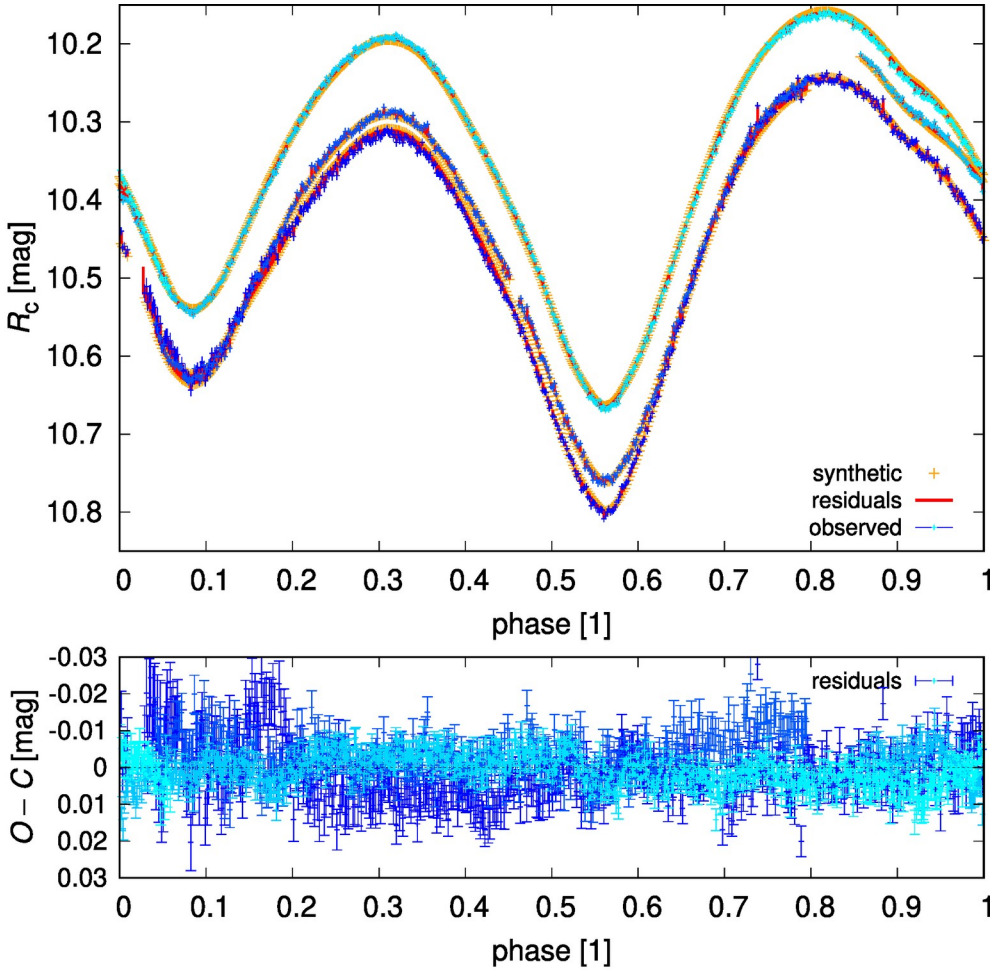

Fig. A.4. Same as Fig. 10, but referring the adjusted shape model of (22) Kalliope. Systematics on the light curves related to the shape were at least partly eliminated. The respective contribution has decreased to $\chi^2_{\rm lc} = 3980$, $n_{\rm lc} = 1829$.

‘Cliptracing’ algorithm

exact synthetic image, pixel = polygon, 3rd clipping: **partial flux-contributions**, no artifacts!

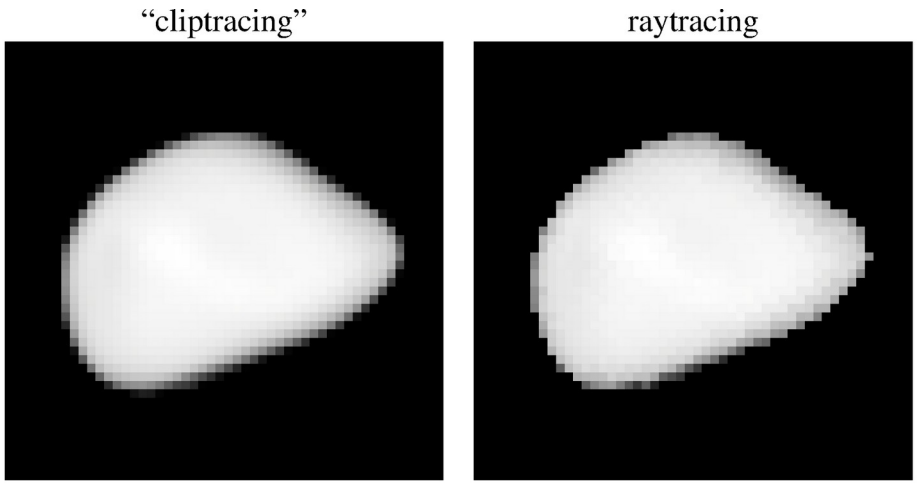

Fig. 4. 1:1 comparison of the ‘cliptracing’ (left) and the raytracing (right) algorithms. In the former, polygons were clipped by individual pixels (analytically) and the synthetic image of (22) is very smooth. In the latter, a simple inside-polygon test was used for each ray, which creates discretisation artefacts and the synthetic image is then ‘noisy’. The Lambert scattering law was used in this test.

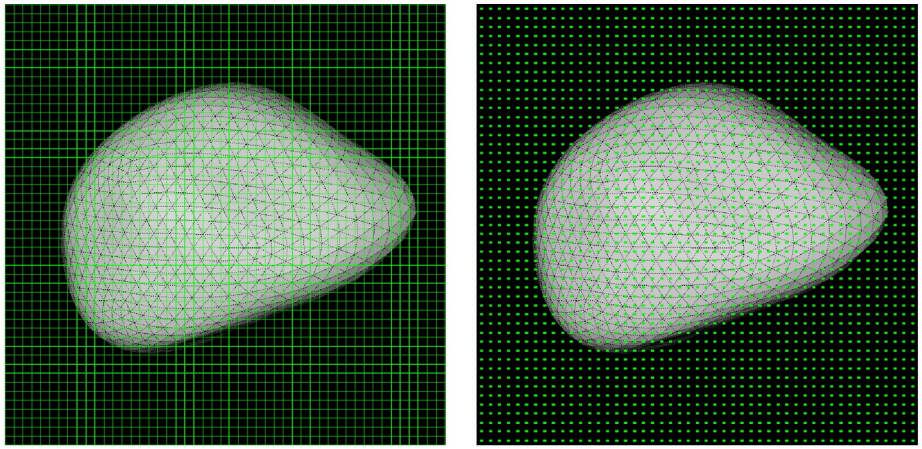

Fig. 5. Same as Fig. 4, but showing the corresponding shape composed of polygonal faces (gray) and a grid of either square pixels or points (green).

```fortran
do i = 1, h
  do j = 1, w

    u = +(dble(j-1)/(w-1)-0.5d0)*w * du + c(1)*d_to
    v = -(dble(i-1)/(h-1)-0.5d0)*h * dv + c(2)*d_to
    r = u*hatu + v*hatv
    u = r(1)
    v = r(2)

    ! 1 pixel as a box
    pxl = (/u-0.5d0*du, u+0.5d0*du, v-0.5d0*dv, v+0.5d0*dv, 0.d0, 0.d0/)

    if ((pxl(2).lt.box1(1)).or.(pxl(1).gt.box1(2))) cycle
    if ((pxl(4).lt.box1(3)).or.(pxl(3).gt.box1(4))) cycle

    ! 1 pixel as a set of polygons
    poly1%c = 1
    poly1%s(1)%c = 4
    poly1%s(1)%p(1,:) = (/pxl(1), pxl(3), 0.d0/)
    poly1%s(1)%p(2,:) = (/pxl(2), pxl(3), 0.d0/)
    poly1%s(1)%p(3,:) = (/pxl(2), pxl(4), 0.d0/)
    poly1%s(1)%p(4,:) = (/pxl(1), pxl(4), 0.d0/)

    tot = 0.d0
    do k = 1, size(polys,1)
      if (polys(k)%c.eq.0) cycle
      if ((pxl(2).lt.boxes(k,1)).or.(pxl(1).gt.boxes(k,2))) cycle
      if ((pxl(4).lt.boxes(k,3)).or.(pxl(3).gt.boxes(k,4))) cycle

      call crop_in_c(polys(k), poly1, polystmp(1))

      if (polystmp(1)%c.eq.0) cycle

! Note: no back-projection of surf => division by mu_e!

      ! i.e., contribution to 1 pixel
      normalstmp(1,:) = normals(k,:)
      S = surface(polystmp, normalstmp, surf)
      tot = tot + Phi_e(k)*S/mu_e(k)
    enddo

    pnm(i,j) = tot

  enddo ! j
enddo ! i
```

residuals
not images
3.6 mas/pxl
rotation
non-trivial

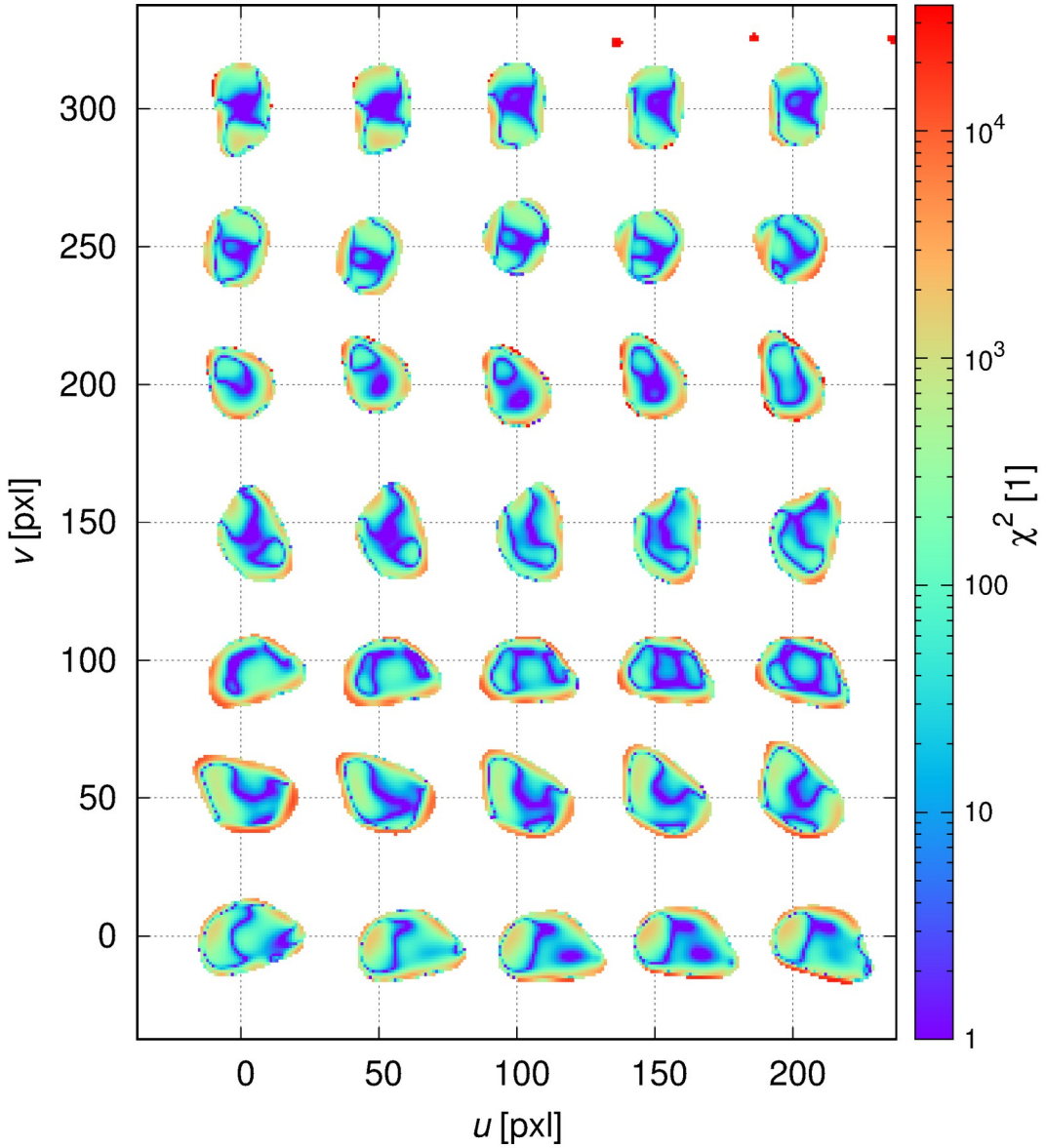

Future work

- applications of Pyshellspec: φ Per, ω CMa
- improving resolution, AMR?
- synthetic images for multiple * in Xitau
- corr. interferometric observables
- complex orbit + shape fitting
- synthetic spectra for fast-rotating *
- synthetic spectra for pulsating *?
- interferometric module for Phœbe?
- non-LTE radiative transfer in CSM?
- ...

Pijl-li žšby kafe taky?